



## Seasonal and mesoscale variability of primary production in the deep winter-mixing region of the NW Mediterranean



Marta Estrada <sup>a,\*</sup>, Mikel Latasa <sup>b</sup>, Mikhail Emelianov <sup>a</sup>, Andrés Gutiérrez-Rodríguez <sup>c</sup>,  
Bieito Fernández-Castro <sup>d</sup>, Jordi Isern-Fontanet <sup>e</sup>, Beatriz Mouriño-Carballido <sup>d</sup>,  
Jordi Salat <sup>a</sup>, Montserrat Vidal <sup>f</sup>

<sup>a</sup> Institut de Ciències del Mar, CSIC, Pg. Marítim de la Barceloneta, 37-49, E-08003 Barcelona, Spain

<sup>b</sup> Instituto Español de Oceanografía, Centro Oceanográfico de Xixón, Camín de l'Arbeyal, s/n, E-33212 Xixón, Spain

<sup>c</sup> Andrés Gutiérrez-Rodríguez, Station Biologique de Roscoff, Place Georges Teissier, 29682 Roscoff cedex, France

<sup>d</sup> Departamento de Ecología y Biología Animal, Universidad de Vigo, Campus universitario Lagoas, Marcosende, E-36310 Vigo, Spain

<sup>e</sup> Institut Català de Ciències del Clima (IC3), C/Doctor Trueta, 203, E-08005 Barcelona, Spain

<sup>f</sup> Departament d'Ecologia, Universitat de Barcelona, Diagonal 643, E-08028 Barcelona, Spain

### ARTICLE INFO

#### Article history:

Received 7 May 2014

Received in revised form

6 August 2014

Accepted 11 August 2014

Available online 27 August 2014

#### Keywords:

Phytoplankton

Chlorophyll *a*

Primary production

NW Mediterranean

Seasonal bloom

Mesoscale

### ABSTRACT

The phytoplankton bloom in the Liguro-Provençal deep convection region represents one of the main fertilization mechanisms in the Mediterranean. This communication examines nano- and microphytoplankton observations, and measurements of primary production and chlorophyll *a* concentration (Chl *a*) in the southwestern part of the deep convection region, where such information is scarce. Data were obtained from four cruises, carried out in 2005 (EFLUBIO project) and 2009 (FAMOSO project), covering the seasonality between mid-March and September in the region. Our aims were to constrain primary production estimates and to ascertain the importance of short-term variability on the photosynthetic response of phytoplankton assemblages during bloom, post-bloom and late-summer stratification periods in the area. Overall, the initial slope of the *P*–*E* relationship ( $\alpha^B$ ) increased and the Chl *a*-normalized photosynthetic rate ( $P_m^B$ ) decreased with increasing optical depth of sample origin, but there were exceptions. In general, there were marked seasonal trends, with stratification increasing and Chl *a* concentration, primary production and dissolved inorganic nitrogen and phosphate fluxes decreasing from winter to late summer. Chl *a* at 5 m depth reached a maximum of 7 mg m<sup>-3</sup> on 25 March 2005, one of the highest values measured in the region. Average surface values ( $\pm$  SD) ranged from respectively 2.4  $\pm$  2.3 mg m<sup>-3</sup> and 2  $\pm$  0.7 mg m<sup>-3</sup> in the March 2005 and March 2009 cruises to 0.12  $\pm$  0.01 mg m<sup>-3</sup> in the September 2009 cruise. Vertically integrated (0–80 m) primary production (PP<sub>int</sub>) attained 1800 mg C m<sup>-2</sup> d<sup>-1</sup> in March 2009, with an average of 1024  $\pm$  523 mg C m<sup>-2</sup> d<sup>-1</sup>, and decreased to a mean of 141  $\pm$  0.43 mg C m<sup>-2</sup> d<sup>-1</sup> in September 2009. Superimposed to the seasonal trends, there was a considerable within-cruise variability of biomass and primary production, especially during the spring-winter bloom and post-bloom periods, when PP<sub>int</sub> could change more than threefold within a few days. These differences were mainly associated with the intense hydrographic mesoscale and sub-mesoscale heterogeneity in the region and with the differences in the physiological and ecological history of the phytoplankton communities inhabiting the different water bodies. In late summer, most PP<sub>int</sub> variability could be explained by fluctuations in surface incident irradiance.

© 2014 Elsevier Ltd. All rights reserved.

### 1. Introduction

Winter mixing is one of the main mechanisms bringing nutrients to the euphotic zone throughout the Mediterranean. However, its intensity and subsequent biological effects present a marked variability. D'Ortenzio and Ribera d'Alcalà (2009) used

SeaWiFS imagery to conclude that, in the open sea, a marked late winter–early spring bloom, typical of a temperate regime, was only observed regularly in the Liguro-Provençal basin of the NW Mediterranean. The cyclonic circulation in this region, together with wind and temperature forcing, favor intense winter convection, which in some years spans all the way to depths exceeding 2000 m and originates the Western Mediterranean Deep Water (MEDOC-Group, 1970; Siokou-Frangou et al., 2010). The development of the phytoplankton bloom in the Ligurian Sea has been described by a number of remote sensing studies (Morel and

\* Corresponding author.

E-mail address: [marta@icm.csic.es](mailto:marta@icm.csic.es) (M. Estrada).

André, 1991; Antoine et al., 1995; Bosc et al., 2004; Morales, 2006), which typically show a period of blue water followed by the appearance of chlorophyll patches in late winter early spring. Years with more intense convection tend to present more phytoplankton biomass due to factors like increased surface nutrient concentrations derived from deeper mixing and the greater spatial extension, duration and recurrence of the mixing events (Volpe et al., 2012; Marty and Chiavérini, 2010). The surface concentration of phytoplankton is reduced by deep mixing, but phytoplankton proliferation may take place as soon as conditions allow growth to exceed losses. The interplay between vertical mixing and phytoplankton bloom development has been modeled by Lévy et al. (1998), who showed the importance of mesoscale features in shaping phytoplankton production.

Although the phytoplankton bloom in the Liguro-Provençal deep convection region (the so-called MEDOC area, between 3° 30' to 6° E and 41° to 43° N, Gascard, 1978) represents one of the main fertilization mechanisms in the Mediterranean (Bosc et al., 2004), most *in situ* measurements of phytoplankton biomass and primary production, based on some oceanographic cruises and the visits to the DYFAMED time series station, have been concentrated on the Ligurian side of the basin (Jacques et al., 1973, 1976; Vidussi et al., 2000; Marty and Chiavérini, 2002; Marty et al., 2008). Primary production data are scarce in the southwestern part of the MEDOC area and there is little information on the characteristics of the photosynthesis-irradiance relationships of the phytoplankton in the region, a knowledge that would enhance our understanding of basic phytoplankton ecophysiology and could help to improve primary production modeling from remote sensing studies. In addition, there are few *in situ* data of the effects of this phytoplankton bloom on the other trophic levels and on the fluxes of carbon through the water column and the atmosphere. Answering this question was the main objective of the FAMOSO project, which included repeated cruises to the southwestern part of the deep convection zone during three periods of 2009 covering winter-spring bloom, post-bloom and late-summer stratification situations. In this paper, we examine primary production data from these surveys and from a previous one carried out in March–April 2005 in the same region. Our aims were to ascertain the importance of seasonal and short-term variability (including both temporal changes in the biological populations and the effects of mesoscale or sub-mesoscale spatial processes) on primary production estimates in the area and on the photosynthetic response of the phytoplankton assemblages. Given the importance of the winter-spring bloom of the NW Mediterranean, knowledge of the C fluxes during this period is a prerequisite to learn whether this region acts as a source or a sink of atmospheric C. In addition, because the NW Mediterranean has been identified as a sensitive region to global change (Somot et al., 2006), information on its biogeochemical and ecological processes is needed for establishing baseline conditions and allowing a reliable assessment of the potential effects of climate change in this marine ecosystem.

## 2. Material and methods

Several oceanographic cruises were conducted in the southwestern part of the Liguro-Provençal Basin, within the region delimited approximately by coordinates 41°30' to 42°N and 4° to 5°E, an area with depths exceeding 2000 m and typically subjected to deep convection in winter (Fig. 1, Table 1). The cruises were carried out on board the R.V. Cornide de Saavedra, in March to early April 2005 [EFLUBIO 2, (E2)], and on board the R. V. Sarmiento de Gamboa in mid-March, late April–May and September 2009 [cruises FAMOSO 1 (F1), FAMOSO 2 (F2) and FAMOSO 3 (F3)], respectively. The sampling strategy intended a Lagrangian approach

by following the track of an array of free drifting Particle Interference Traps deployed during 24 h (EFLUBIO) or 72 h (FAMOSO). Thus, the within-cruise spatial variability observed in our time series reflects both changes in the position of the stations and in the hydrographical fields.

### 2.1. Satellite imagery

Sea Surface Temperature (SST) was obtained from nighttime measurements done by the AVHRR sensor on board the NOAA-18 platform and provided by the SAIDIN facility at the Institut de Ciències del Mar (<http://coo.icm.csic.es/content/saidin-and-thredds>). Brightness Temperature (BT) from channel 4 was used to derive a new SST field instead of using the original SST, with the objective of reducing the noise (e.g. Isern-Fontanet and Hascoët, 2014). The bias associated with the lack of atmospheric correction in the BT field was addressed through linear filtering between the BT and the SST fields and, then, both fields were compared to verify that no spurious structures were introduced by this procedure. The Chl *a* field was derived from measurements done by the MODIS sensor on board the Aqua platform using the OC3M-547 algorithm. The data were downloaded from the NASA's Ocean Color server (<http://oceancolor.gsfc.nasa.gov/>). We used Level 1B (AVHRR) and Level 2 (AVHRR and MODIS) products with the objective to keep the full spatial resolution of the original measurements.

### 2.2. Hydrography

Several CTD casts were carried out each day (except for some gaps due to bad weather) within the same area, at varying positions following the track of the free drifting traps. Vertical profiles of temperature, salinity, oxygen concentration and *in vivo* fluorescence were obtained from all the casts with a CTD SBE 911plus equipped with additional sensors of dissolved oxygen concentration, turbidity, fluorescence, light transmission, irradiance (PAR), surface irradiance (SPAR) and bottom proximity (altimeter). Water from selected depths was collected from a daily “biological” cast (or “station”) starting around 8 GMT, by means of 12 L Niskin bottles mounted on a rosette, and samples were taken for determination of major nutrient and chlorophyll *a* (Chl *a*) concentrations, phytoplankton examination and primary production measurements. On one occasion (station F1-74, see Table 1 for station codes), water for the 24 h on-deck incubations was collected from an additional cast carried out three hours later. Incident irradiance was measured continuously with a LI-200 2πLi-Cor pyranometer. Daily incident irradiance just under the water surface ( $\text{mol photons m}^{-2} \text{d}^{-1}$ ) was estimated from the pyranometer records using an empirical conversion expression (obtained comparing pyranometer readings with a cosine PAR sensor deployed overboard). Water-column downward PAR (400–700 nm) was measured around noon at each station with a spherical quantum sensor mounted on a FRRF instrument. The vertical light extinction coefficients ( $K_d$ ) were obtained from the regression of  $\log(\text{PAR})$  versus depth ( $z$ ) for the whole upper water column, or for adjoining layers above ( $K_{ds}$ ) and below ( $K_{dp}$ ) the deep chlorophyll maximum (DCM) when changes in the slope of the plots were detected. Optical depths (OD) for a depth  $z$  were calculated as the product of  $K_d z$  or as  $K_{ds} z_{\text{DCM}} + K_{dp}(z - z_{\text{DCM}})$ , where  $z_{\text{DCM}}$  is the DCM depth, when  $z > z_{\text{DCM}}$  and different light extinction coefficients had been determined for layers above and below the DCM. The mixed layer depth was estimated as the first depth ( $z$ ) for which  $\sigma_\theta(z) - \sigma_\theta(5) \geq 0.125 \text{ kg m}^{-3}$ , where  $\sigma_\theta(z)$  and  $\sigma_\theta(5)$  are, respectively, the potential density anomalies at depths  $z$  and 5 m. A vertical stratification index (VSI), between 5 and 80 m depth, was calculated as  $\sum(\sigma_\theta(z+1) - \sigma_\theta(z))$ , where  $z$  is the depth in m and ranges from 5 to 79.

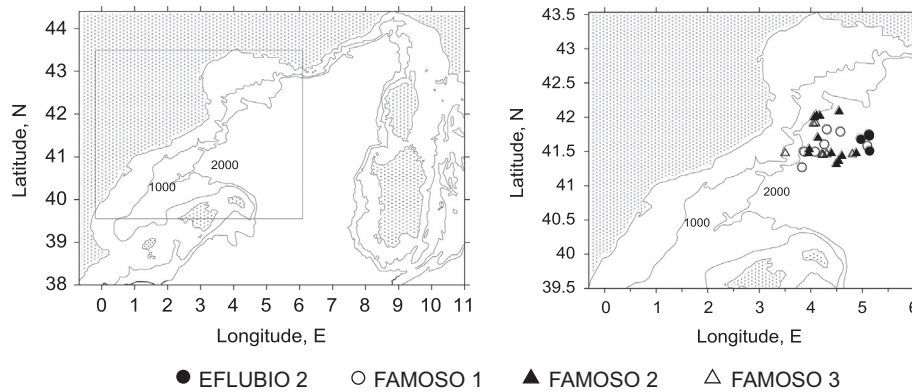


Fig. 1. Map of the NW Mediterranean (A) and inset showing the position of the biological stations (B).

Table 1

Date, cast number, year day, code, position and environmental information of the biological stations of the cruises EFLUBIO 2, FAMOSO 1, FAMOSO 2 and FAMOSO 3.  $t$ : temperature ( $^{\circ}\text{C}$ ) at 5 m depth,  $S$ : salinity at 5 m depth,  $H_0$ : total daily incident irradiance at the water surface ( $\text{mol photons m}^{-2} \text{d}^{-1}$ ),  $Z_{\text{uml}}$ : upper mixed layer depth (m),  $Z_{\text{eu}}$ : euphotic zone depth (m), VSI: stratification index (see Section 2.2).

Cruise/date	CTD cast	Year day	Station code	$^{\circ}\text{N}$	$^{\circ}\text{E}$	$t^{\circ}\text{C}$ at 5 m	$S$ at 5 m	$H_0$	$Z_{\text{uml}}$ (m)	$Z_{\text{eu}}$ (m)	VSI	
<b>EFLUBIO 2 (E2)</b>												
3/25/2005	83	84	E2-84	41 45.01	5 7.59	13.66	38.416	14.4	26	18.8	0.20	
3/26/2005	91	85	E2-85	41 30.97	5 8.03	13.56	38.422	14.5	22	25.8	0.19	
3/27/2005	99	86	E2-86	41 44.23	5 7.82	13.62	38.419	38.3	25	48.2	0.28	
3/28/2005	109	87	E2-87	41 44.96	5 7.61	13.47	38.293	35.8	40	45.4	0.22	
3/29/2005	118	88	E2-88	41 44.29	4 57.79	13.56	38.345	27.6	37	46.5	0.24	
4/5/2005	166	95	E2-95	41 45.29	5 7.44	14.10	38.332	36.4	14	49.3	0.47	
						Mean	13.66	38.371	27.8	27.3	39.0	0.27
						SD	0.22	0.055	11.0	9.7	13.2	0.10
<b>FAMOSO 1 (F1)</b>												
3/14/2009	13	73	F1-73	41 35.19	5 5.53	13.14	38.250	39.4	60	38.4	0.14	
3/15/2009	15	74	F1-74	41 30.18	3 51.74	13.09	38.249	37.4	68	40.8	0.16	
3/18/2009	21	77	F1-77	41 30.05	4 4.50	13.22	38.338	44.3	43	35.0	0.14	
3/19/2009	24	78	F1-78	41 36.46	4 15.43	13.31	38.298	38.0	65	34.2	0.18	
3/21/2009	27	80	F1-80	41 49.62	4 18.31	13.17	38.354	37.7	> 200	41.5	0.11	
3/22/2009	31	81	F1-81	41 47.61	4 34.13	13.05	38.374	39.7	> 200	42.9	0.06	
						Mean	13.16	38.311	39.4	59.0	38.8	0.13
						SD	0.10	0.053	2.6	11.2	3.6	0.04
<b>FAMOSO 2 (F2)</b>												
4/30/2009	5	120	F2-120	41 0.01	04 52.44	14.41	38.249	42.5	41	59.8	0.42	
5/3/2009	11	123	F2-123	41 09.95	03 56.36	14.89	38.109	48.9	40	62.8	0.61	
5/4/2009	15	124	F2-124	41 03.45	03 57.46	15.11	38.124	38.6	24	62.5	0.60	
5/7/2009	20	127	F2-127	42 06.60	04 32.42	14.57	38.321	49.8	51	67.2	0.36	
5/8/2009	26	128	F2-128	42 01.54	04 03.58	15.18	38.268	40.6	25	96.7	0.52	
5/9/2009	30	129	F2-129	42 03.26	04 05.90	15.34	38.271	39.3	15	68.5	0.56	
5/10/2009	32	130	F2-130	42 02.83	04 09.90	15.60	38.275	35.3	15	86.3	0.65	
5/11/2009	36	131	F2-131	41 27.58	04 35.78	16.05	38.280	53.7	12	68.7	0.72	
5/12/2009	40	132	F2-132	41 24.51	04 32.68	16.12	38.274	34.7	16	69.1	0.72	
5/13/2009	44	133	F2-133	41 20.34	04 29.17	16.54	38.258	41.1	14	68.7	0.76	
						Mean	15.38	38.243	42.4	25.3	71.0	0.59
						SD	0.70	0.069	6.3	13.9	11.5	0.13
<b>FAMOSO 3 (F3)</b>												
9/16/2009	5	259	F3-259	41 28.59	4 18.44	24.00	38.168	12.6	29	78.2	4.04	
9/17/2009	8	260	F3-260	41 28.42	4 13.79	23.92	38.193	16.8	34	83.1	2.71	
9/18/2009	12	261	F3-261	41 28.59	4 12.46	23.90	38.178	37.7	28	82.8	3.02	
9/19/2009	15	262	F3-262	41 55.76	4 2.67	22.69	38.226	21.8	28	61.3	2.62	
9/20/2009	20	263	F3-263	41 56.22	4 5.14	23.68	38.193	28.7	24	—	2.90	
						Mean	23.64	38.192	23.5	28.6	76.4	3.06
						SD	0.54	0.022	10.0	3.6	10.3	0.57

### 2.3. Nutrient analyses, nutrient fluxes and chlorophyll *a* determinations

Dissolved inorganic phosphorus ( $\text{PO}_4^{3-}$ , DIP) was determined spectrophotometrically on board, using a 10 cm cuvette to increase the detection limit to  $0.01 \text{ mmol m}^{-3}$ , while water samples for the determination of dissolved inorganic nitrogen

( $\text{NO}_3^- + \text{NO}_2^-$ , DIN) and silicate ( $\text{SiO}_4^{3-}$ ) were frozen for later analysis on land with an AA3 autoanalyzer. Silicate determinations failed and are unavailable for FAMOSO samples. Methods were as described in Grasshoff et al. (1999).

Measurements of turbulent kinetic energy dissipation ( $\varepsilon$ ) were carried out in the FAMOSO cruises by means of a microstructure turbulence profiler (Prandke and Stips, 1998) and were used to

estimate the vertical turbulent diffusivity. On average, 7 microstructure profiles were performed in each station down to a depth of about 250–300 m, with a vertical resolution of 1 m. A single profile of the vertical diffusivity ( $K_z$ ) was generated for each station in a 10 m grid as

$$K_z = \Gamma \frac{(\epsilon)_{10\text{ m}}}{N^2}$$

where  $\Gamma=0.2$  (Osborn, 1980) is a mixing efficiency and  $N^2$  is the squared buoyancy frequency computed by linear fitting of the slope of the density profile in 10 m bins. A detailed description of the microstructure profiler and the data processing is included in Mourão-Carballido et al. (2011). Nutrient (DIN or DIP) fluxes ( $F_{\text{nut}}$ ) were computed as the product of the slope of the nutricline ( $d[\text{nut}]_{\text{nutricline}}/dz$ ), obtained by linear fitting of the nutrient concentrations, and the averaged diffusivity for the same depth range:

$$F_{\text{nut}} = -(K_z)_{\text{nutricline}} \frac{d[\text{nut}]_{\text{nutricline}}}{dz}$$

Samples for Chl *a* determination were generally collected from 4 to 8 levels between 5 and 100 m. For Chl *a* analysis, between 50 and 200 ml of seawater were filtered through Whatman GF/F filters, which were stored at  $-20^\circ\text{C}$  during several hours and subsequently introduced into 90% acetone for 24 h extraction in the dark. The fluorescence of the acetonic extract was determined with a Turner Designs fluorometer (Yentsch and Menzel, 1963); no phaeophytin corrections were applied because of the uncertainties of the method (Welshmeyer, 1994). In order to calculate integrated Chl *a* in the water column between 0 and 80 m ( $\text{Chl } a_{\text{int}}$ ,  $\text{mg Chl } a \text{ m}^{-2}$ ), Chl *a* concentration between 0 and 5 m depth was assumed to be equal to Chl *a* concentration at 5 m and, below this depth, when the interval between samples exceeded 10 m, Chl

*a* concentrations at intermediate depths (typically at 10 m intervals) were interpolated according to the following procedure. First, a linear interpolation was performed, based on the closest available Chl *a* determinations above and below the interpolation depth. In a similar way, a linear interpolation was also carried out for the CTD *in vivo* fluorescence data corresponding to the same depths. Next, the interpolated Chl *a* concentration value calculated for the interpolation depth was multiplied by the ratio between the actually recorded fluorescence and the lineally interpolated fluorescence for this depth. This correction factor was introduced to compensate for deviations from linearity of the Chl *a* profile and was based on the assumption that *in vivo* fluorescence would be linearly proportional to Chl *a* concentration across subsurface depth intervals  $< 30$  m. As different fluorescence sensors were used, to make fluorescence units roughly comparable among cruises, the fluorescence values shown in Figs. 2–3, 5 and 6 were transformed using a regression equation of measured Chl *a* on fluorescence for each cruise.

#### 2.4. Phytoplankton examination

Phytoplankton samples were taken from the same depths as the primary production experiments; a volume of 150 ml was placed in glass bottles and fixed with formalin–hexamine solution. The phytoplankton was enumerated by means of the inverted microscope technique (Estrada et al., 1999), after sedimentation of 100 ml of sample in composite settling chambers. This method is not adequate for small organisms in the picophytoplankton size range; therefore, our observations concern nano and microphytoplankton, although, for simplicity, we will use the term “phytoplankton” when referring to them in the text.

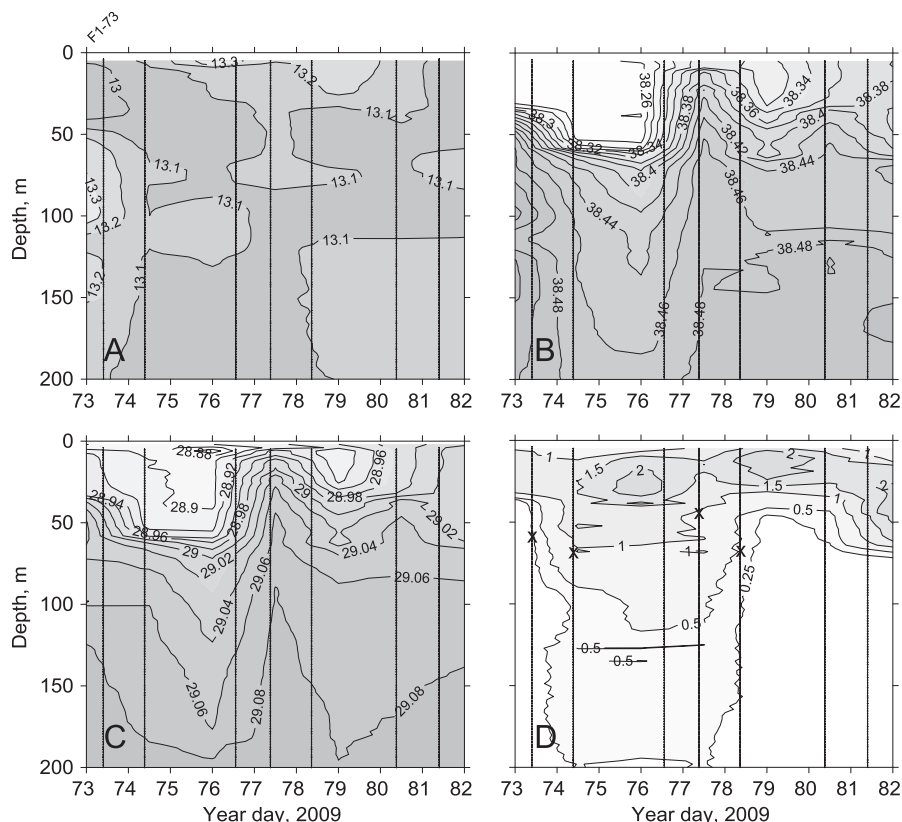


**Fig. 2.** Cruise FAMOSO 1 (F1). Temporal evolution of (A) temperature, (B) salinity, (C) potential density anomaly and (D) *in vivo* fluorescence. The vertical lines indicate CTD profiles. The “x” in D indicates the upper mixed layer depth (in the last two stations, it exceeded 200 m).

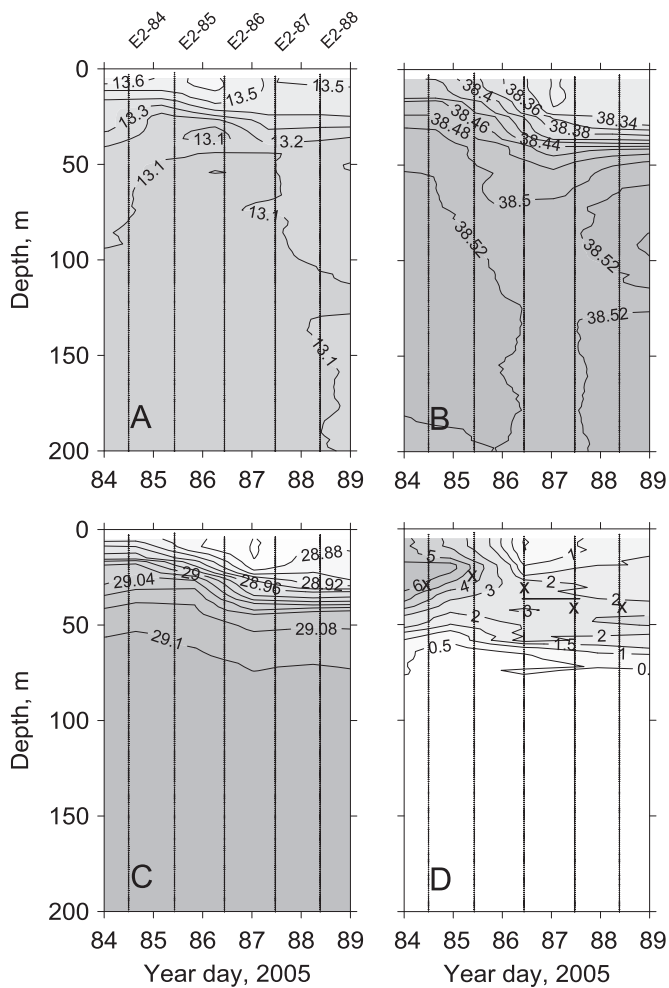


**Fig. 3.** Cruise EFLUBIO 2 (E2). Temporal evolution of (A) temperature, (B) salinity, (C) potential density anomaly and (D) *in vivo* fluorescence. The vertical lines indicate CTD profiles. The “x” in D indicates the upper mixed layer depth.

### 2.5. Photosynthesis–irradiance (*P*–*E*) experiments

Water for these experiments was taken from the surface (generally 5 m depth) and from a deeper level coinciding with the Chl *a* maximum, when it existed. For brevity, the deep sample will be designated as the DCM (deep chlorophyll maximum) sample, although the Chl *a* maximum occurred at surface or was close to it in F1 (between 5 and 20 m depth). For each depth, 14 tissue bottles (one of them, the “dark” bottle, wrapped with aluminum foil) were filled with 70 ml of water, inoculated with  $\sim 3.7 \times 10^5$  Bq  $^{14}\text{C}$ -bicarbonate and incubated for 2 h in lineal incubators, with circulating surface water for the 5 m incubator and with refrigerated water at *in situ* temperature for the DCM incubator. Illumination was provided by means of halogen lamps; neutral screens were placed between some of the bottles, to ensure a PAR gradient of 0 to  $730\text{--}1200 \mu\text{mol photons m}^{-2} \text{s}^{-1}$ . Irradiance levels at each position were measured after each experiment with a cosine quantum sensor (Li-Cor LI-190SZ or an Illuminova sensor previously calibrated with the Li-Cor). After incubation, samples were filtered onto Whatman GF/F filters (25 mm diameter), which were placed in 6 ml scintillation vials and fumed overnight with 35% HCl. Radioactivity was measured by means of a Beckman LS6500 liquid scintillation counter, after addition of Ready Safe cocktail to the vials. Ambient inorganic carbon concentration was assumed to be  $25,000 \text{ mg C m}^{-3}$  (Morán and Estrada, 2005).

The models of Platt et al. (1980) or Webb et al. (1974) were fitted to the Chl *a*-normalized hourly carbon fixation rates depending, respectively, on whether photoinhibition was detected or not. The derived photosynthetic parameters were  $P_m^B$ , the light-saturated Chl *a*-normalized photosynthetic rate [ $\text{mg C (mg Chl } a)^{-1} \text{ h}^{-1}$ ],  $\alpha^B$ , the initial slope of the *P*–*E* relationship [ $\text{mg C (mg Chl } a)^{-1} (\mu\text{mol photons m}^{-2} \text{ s}^{-1})^{-1} \text{ h}^{-1}$ ] and  $\beta^B$ , the photoinhibition parameter (same units as  $\alpha^B$ ). The photoacclimation parameter,  $E_k$  ( $\mu\text{mol photons m}^{-2} \text{ s}^{-1}$ ) was calculated as the quotient between  $P_m^B$  and  $\alpha^B$ . For each station, the C fixation data from the *P*–*E* curves and the depth profiles of PAR and Chl *a* were used to estimate the daily rates of primary production at different depths of the water column. Integrated primary production values between surface and 80–100 m depth ( $\text{PP}_{\text{int}}$ ,  $\text{mg C m}^{-2} \text{ d}^{-1}$ ) were calculated by the trapezoidal method, as described in Morán and Estrada (2005). The same model was used to calculate the daily primary production values at nominal light depths coinciding with those used for the on-deck incubations (see Section 2.6). A rough estimate of the relative importance of fluctuations in irradiance due to variable cloud cover (“original” irradiance conditions) for within-cruise  $\text{PP}_{\text{int}}$  variability was obtained by recalculating the values of  $\text{PP}_{\text{int}}$ . For that we used the same daily incident irradiance values (those of one of the sunny days) for all the stations of the same cruise (“sunny-day” irradiance conditions) and compared the coefficients of variation of the “original” and “sunny-day” irradiance conditions  $\text{PP}_{\text{int}}$  estimates.

### 2.6. On-deck 24 h incubations for C uptake determination

In addition to the 2 h *P*–*E* experiments, we performed  $^{14}\text{C}$  uptake experiments on-deck with natural irradiance. The incubator consisted of a rectangular container with 10 Perspex cylinders, wrapped in blue screens to provide a range of attenuation of the incoming PAR, and supplied with a continuous flow of surface seawater regulated by a Julabo FC1200 recirculating cooler to mimic the *in situ* temperature of the samples (Table 2). Two series of 20 tissue bottles of 70 ml were filled, one with water from 5 m depth and another with water from the DCM, and inoculated with  $\sim 3.7 \times 10^5$  Bq  $^{14}\text{C}$ -bicarbonate. Two replicate bottles from surface and two from the DCM, plus the corresponding dark controls, were placed in each cylinder and incubated during 24 h. Care was taken to avoid the effect of ambient light on the bottles, by covering them during manipulations. The rates of carbon fixation for station F2-129 appeared to be abnormally low, relative to Chl *a*, when compared with those of the previous and following stations and were excluded from the regression calculations. The major axis regression lines used in the comparison between C fixation rates derived from *P*–*E* curves and from on-deck incubations were fitted using the SMATR software (Falster, et al., 2006).

## 3. Results

### 3.1. Hydrography and phytoplankton

The two winter–early spring cruises E2 (2005) and F1 (2009) presented fairly homogeneous or weakly stratified profiles of temperature, salinity and potential density anomaly ( $\sigma_t$ ), as a result of winter mixing (Figs. 2, and 3). There was considerable mesoscale and submesoscale hydrographical variability in the region, as can be observed in both the SST and Chl *a* distributions shown in Fig. 4A–C. During F1, the interweaving of relatively cool and high salinity waters with more stratified regions of low salinity surface water caused abrupt changes in the hydrographical structure of the upper water column (e.g., year days 77–78 in Fig. 2). The E2 series shows two different situations, with a transition towards increased

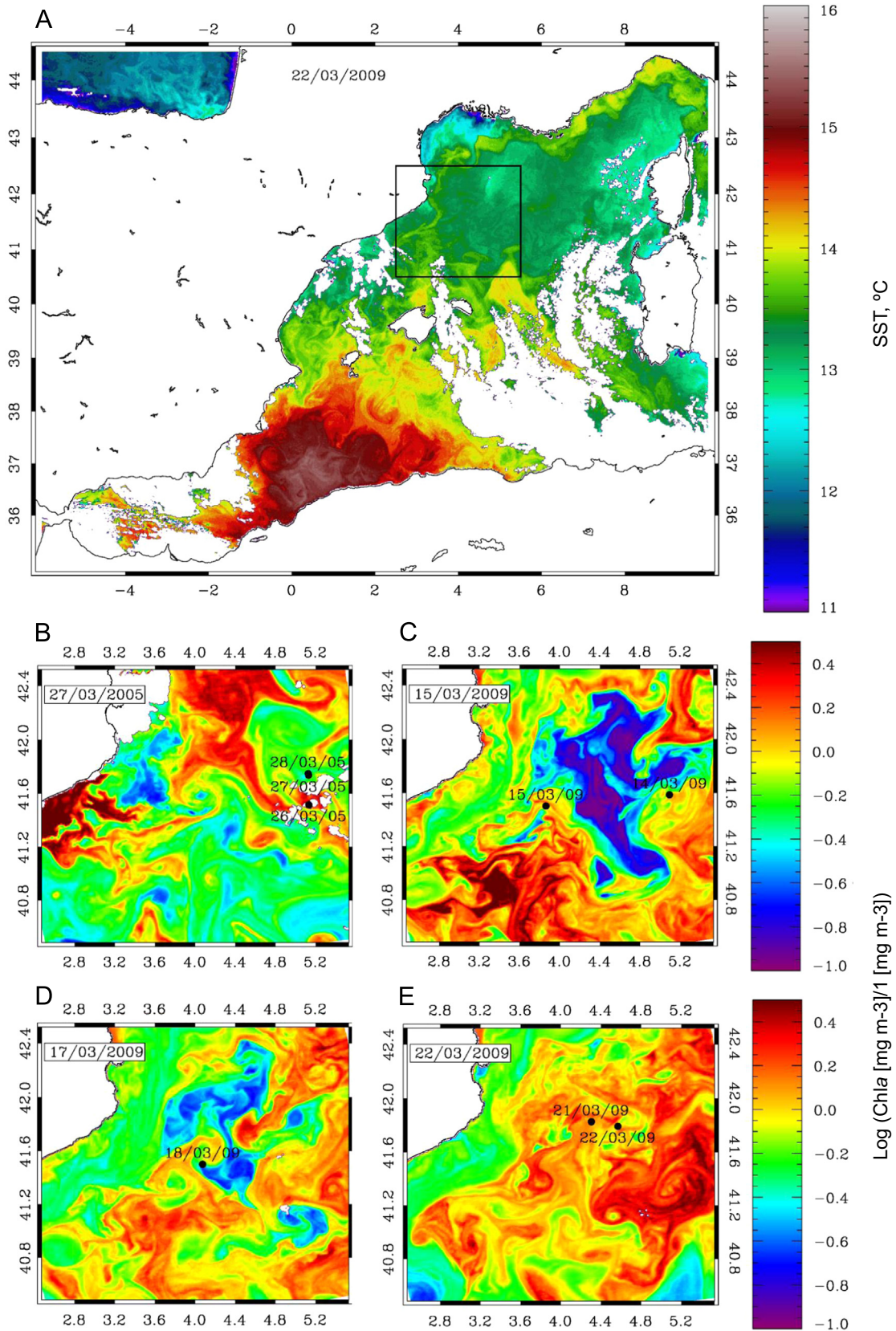


**Fig. 4.** Remote-sensing derived images. (A) Sea Surface Temperature in the W Mediterranean on 22 March 2009. (B–E) Chl a on different dates during cruises E2 and F1 [region marked with a square in (A)]: 27 March 2005 (B), 15 March 2009 (C), 17 March 2009 (D) and 22 March 2009 (E). Note that the Chl a scale is logarithmic. The black circles and dates in B–E indicate the position and date of stations carried out within two days of the image observation.

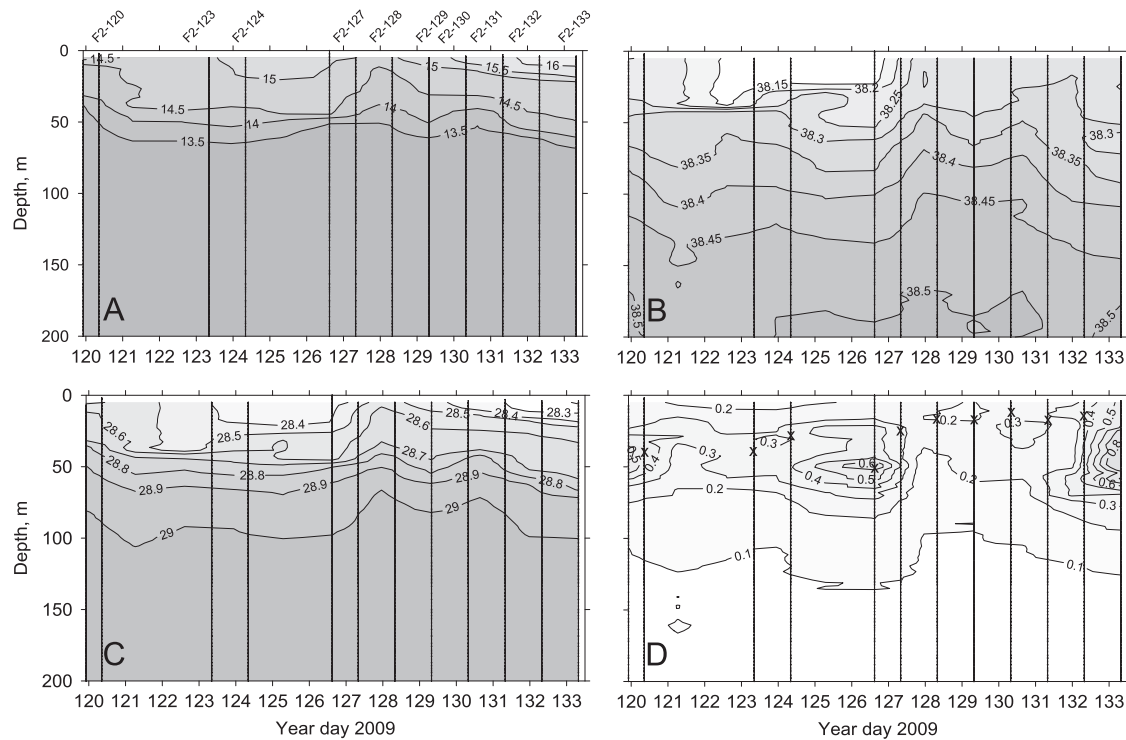


**Fig. 5.** Cruise FAMOSO 2 (F2). Temporal evolution of (A) temperature, (B) salinity, (C) potential density anomaly and (D) *in vivo* fluorescence. The vertical lines indicate CTD profiles. The “x” in D indicates the upper mixed layer depth.

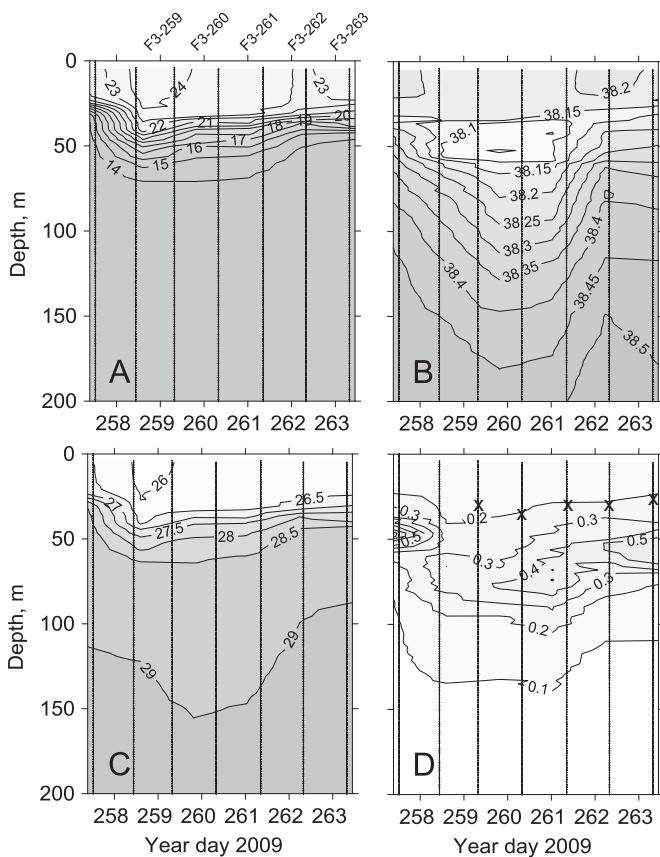


**Fig. 6.** Cruise FAMOSO 3 (F3). Temporal evolution of (A) temperature, (B) salinity, (C) potential density anomaly and (D) *in vivo* fluorescence. The vertical lines indicate CTD profiles. The “x” in D indicates the upper mixed layer depth.

**Table 2**

Percentage of surface incident irradiance in the incubators used in the 24 h on-deck <sup>14</sup>C fixation experiments.

Incubator number	FAMOSO 1	FAMOSO 2	FAMOSO 3
1	32.07	46.47	39.81
2	18.95	39.61	30.19
3	13.78	24.33	20.00
4	13.28	18.57	10.53
5	9.00	15.31	6.96
6	6.97	8.00	3.71
7	6.73	3.32	2.87
8	4.85	2.63	1.69
9	3.71	1.80	1.44
10	0.00	0.00	0.00

stratification linked to higher temperature and lower salinity at surface after year day 86 (Fig. 3, Table 1). Average concentrations of DIN and DIP ( $\pm$ SD) for surface samples (between 0 and 10 m depth) were, respectively,  $4.47 \pm 1.18 \text{ mmol m}^{-3}$  and  $0.11 \pm 0.06 \text{ mmol m}^{-3}$  for F1, and  $1.41 \pm 0.64 \text{ mmol m}^{-3}$  and  $0.02 \pm 0.01 \text{ mmol m}^{-3}$  for E2. Surface silicate concentrations during E2 averaged  $0.79 \pm 0.36 \text{ mmol m}^{-3}$  (silicate concentrations were not available for the FAMOSO cruises). Both F1 and E2 took place during the phytoplankton bloom period, as evidenced by surface Chl *a* exceeding  $1 \text{ mg m}^{-3}$  (Table 3). During F1, the Chl *a* concentration was fairly homogeneous from the surface down to 20 m (as at stations F1-73 and F1-80 on 14 and 21 March 2009), and 60–80 m [as at stations F1-74, F1-77 and F1-81, on 15, 18 and 22 March respectively (Fig. 7A)]. The maximum Chl *a* concentration reached during this cruise (about  $3 \text{ mg m}^{-3}$ ) was measured on 19 March, (F1-78) at 5 m depth. During E2, Chl *a* concentration at the surface reached values of  $7 \text{ mg m}^{-3}$  (station E2-84), the highest value recorded during this study, and declined with the

**Table 3**  
Cruises EFLUBIO 2 (E2), FAMOSO 1 (F1), FAMOSO 2 (F2) and FAMOSO 3 (F3). Station codes (cruise-year day); sampling depths of on deck incubations; sampling depths, photosynthetic parameters and Chl *a* concentrations for the surface (Chl  $a_s$ ) and DCM (Chl  $a_{DCM}$ ) samples of the *P-E* experiments; integrated Chl *a* concentration (Chl  $a_{int}$ ) and primary production ( $PP_{int}$ ) between 0 and 80 m depth. Also shown are mean and standard deviations (SD) of the parameters for each cruise.  $\alpha^B$ : slope of the *P-E* relationship [ $\text{mg C}(\text{mg Chl } a)^{-1}(\mu\text{mol photons m}^{-2} \text{s}^{-1})^{-1} \text{h}^{-1}$ ],  $P_m^B$ : maximum chlorophyll *a*-normalized photosynthetic rate, [ $\text{mg C}(\text{mg Chl } a)^{-1} \text{h}^{-1}$ ],  $\beta^B$ : photoinhibition parameter (same units as  $\alpha^B$ ),  $E_k$ : light saturation parameter ( $\mu\text{mol photons m}^{-2} \text{d}^{-1}$ ).

Station code	On deck						DCM samples								
	Depth (m)	Depth (m)	Chl $a_s$ ( $\text{mg m}^{-3}$ )	$\alpha^B$	$P_m^B$	$\beta^B$	$E_k$	Depth (m)	Chl $a_{DCM}$ ( $\text{mg m}^{-3}$ )	$\alpha^B$	$P_m^B$	$\beta^B$	$E_k$	Chl $a_{int}$ ( $\text{mg m}^{-2}$ )	$PP_{int}$ ( $\text{mg C m}^{-2} \text{d}^{-1}$ )
E2-84 <sup>a</sup>		5	6.86	0.0028	---	---	40	2.72	0.0022	---	---		259.5	199	
E2-85 <sup>a</sup>		5	2.00	0.0056	1.18	---	211	20	6.07	0.0035	0.54	---	154	231.4	208
E2-86		5	0.46	0.0079	4.31	---	545	40	1.97	0.0065	4.19	0.001	640	69.1	365
E2-87		5	2.03	0.0035	2.28	---	651	50	3.80	0.0037	0.63	---	171	146.1	487
E2-88		5	1.85	0.0032	4.45	---	1391	50	2.66	0.0033	1.18	---	358	131.0	484
E2-95		17.7	1.19	0.0130	4.48	---	345	50.7	1.82	0.0126	2.85	0.0003	226	111.4	755
Mean			2.40	0.0060	3.34		629		3.17	0.0053	1.88		310	158.1	417
SD			2.27	0.0039	1.52		459		1.58	0.0039	1.59		201	73.0	209
F1-73		5	1.46	0.0104	2.71	---	260	20	1.20	0.0105	2.64	---	252	51.2	465
F1-74 <sup>a</sup>	20	5	1.16	0.0143	2.67	---	187	25	1.40	0.0095	3.31	---	349	92.6	646
F1-77	5	5	1.67	0.0078	4.47	---	572	20	1.47	0.0109	3.86	---	355	97.5	672
F1-78	5	5	2.98	0.0141	3.23	---	229	15	2.91	0.0139	2.86	---	206	111.9	1132
F1-80	5	5	2.33	0.0124	4.93	---	399	15	2.53	0.0125	3.38	---	271	84.6	1411
F1-81		5	2.33	0.0154	5.89	---	382	15	2.33	0.0169	5.25	---	310	159.6	1817
Mean			1.99	0.0124	3.98		338		1.97	0.0124	3.55		290	99.6	1024
SD			0.68	0.0028	1.32		142		0.70	0.0027	0.94		59	35.7	523
F2-120	5	5	0.42	0.0060	1.73	---	290	25	0.43	0.0114	2.19	---	192	27.8	191
F2-123	5	5	0.26	0.0101	3.89	---	384	40	0.38	0.0136	3.24	---	239	21.2	280
F2-124	5	5	0.33	0.0104	4.07	---	392	30	0.42	0.0181	3.08	---	170	24.5	349
F2-127	5	5	0.52	0.0101	2.30	---	228	30	0.27	0.0271	4.56	---	168	20.6	504
F2-128	5	5	0.45	0.0102	2.57	---	252	38	0.25	0.0189	1.84	---	97	17.7	336
F2-129	5	5	0.38	0.0098	3.48	---	354	45	0.28	0.0381	4.69	---	123	20.4	294
F2-130	5	5	0.51	0.0120	3.70	---	307	20	0.38	0.0162	3.49	---	215	21.0	422
F2-131	5	5	0.60	0.0134	4.67	---	349	55	0.36	0.0276	3.97	---	144	27.1	643
F2-132	5	5	0.69	0.0101	5.05	---	502	58	0.54	0.0185	2.41	---	130	36.9	580
F2-133		5	0.85	0.0116	3.31	---	286	50	0.98	0.0226	1.52	---	67	64.7	881
Mean			0.50	0.0104	3.47		334		0.43	0.0212	3.10		155	28.2	448
SD			0.18	0.0019	1.04		80		0.21	0.0079	1.10		53	13.9	207
F3-259	5	5	0.14	0.0147	2.69	---	184	80	0.77	0.0255	0.33	0.001	13	27.1	106
F3-260	5	5	0.10	0.0118	3.10	---	264	85	0.45	0.0257	0.47	0.001	18	20.0	95
F3-261	5	5	0.11	0.0125	2.63	---	211	75	0.44	0.0176	0.59	0.001	34	22.0	184
F3-262		5	0.12	0.0193	3.38	---	176	60	0.68	0.0178	1.90	0.004	107	25.0	134
F3-263		5	0.13	0.0197	4.65	---	236	60	0.75	0.0139	1.28	0.002	92	27.1	186
Mean			0.12	0.0156	3.29		214		0.62	0.0201	0.91	0.002	53	24.3	141
SD			0.01	0.0037	0.82		37		0.16	0.0053	0.66	0.001	44	3.2	43

<sup>a</sup> The Chl *a* data used for the Chl  $a_{int}$  calculation were taken from an additional CTD cast.

stratification increase observed towards the end of the cruise, which was accompanied by the appearance of a DCM around 40 m depth (Figs. 3 and 7C). The cooler surface temperatures and the lower stratification during F1 (Table 1, Figs. 2–3), carried out in mid-March, indicate that this cruise corresponds both to an earlier calendar date and a prior phase of the seasonal stratification cycle than E2, that took place in late March. Satellite imagery of both cruises showed highly heterogeneous Chl *a* distributions and a Chl *a*-poor area, corresponding to the deep convection region, which became progressively smaller as the season advanced (Fig. 4B–E).

The F2 cruise, carried out between the end of April 2009 and mid-May (post-bloom period), revealed nearly homogeneous mixed layers of about 50 m in some of the stations (F2-120, F2-123 and F2-127) and continuous or two-step density profiles, with strong additional gradients around 12–25 m depth, at the other stations (Fig. 5, Table 1). This vertical structure of the biological casts (sampled around 8:00 GMT) was similar to that of other casts carried out on the same day before dawn, so that it could not be attributed to daily warming. A rising of the isotherms and isohalines of the upper water layer around 7–8 April (Julian days 127–128) indicated the crossing of a front (Fig. 5). Average surface DIN and

DIP concentrations were, respectively,  $1.77 \pm 0.97 \text{ mmol m}^{-3}$  and  $0.03 \pm 0.02 \text{ mmol m}^{-3}$ . Chl *a* increased substantially in the last stations (to a maximum value of  $1.1 \text{ mg m}^{-3}$  at station F2-133) and was fairly homogenous down to 40–50 m depth in the first samplings and to 70–80 m depth in the last ones (Figs. 5 and 7E).

During F3 (September 2009), the water column was strongly stratified (Table 1) with a surface mixed layer of  $\sim 30$  m and a salinity minimum below it, at  $\sim 35$ –60 m depth (Fig. 6). Just under the strong pycnocline, there was a marked DCM at 60–80 m depth (Fig. 6), and a deep oxygen maximum at slightly shallower levels (data not shown). Surface DIN and DIP concentrations were, on average,  $1.48 \pm 0.53 \text{ mmol m}^{-3}$  and  $0.03 \pm 0.01 \text{ mmol m}^{-3}$ , and Chl *a* concentration fluctuated between 0.10 and  $0.14 \text{ mg m}^{-3}$  at 5 m depth and between 0.4 and  $0.8 \text{ mg m}^{-3}$  at the DCM (Figs. 6 and 7G).

Integrated Chl *a* between 0 and 80 m (Table 3) ranged from around  $20 \text{ mg m}^{-2}$  in some samplings of April–May and September 2009 to more than  $200 \text{ mg m}^{-2}$  in the winter cruises (up to maxima of  $160 \text{ mg m}^{-2}$  in March 2009 and  $260 \text{ mg m}^{-2}$  in March 2005). There was an overall significant linear relationship between surface and integrated Chl *a* ( $r=0.85$ ,  $p < 0.01$ ,  $n=27$ ), but with

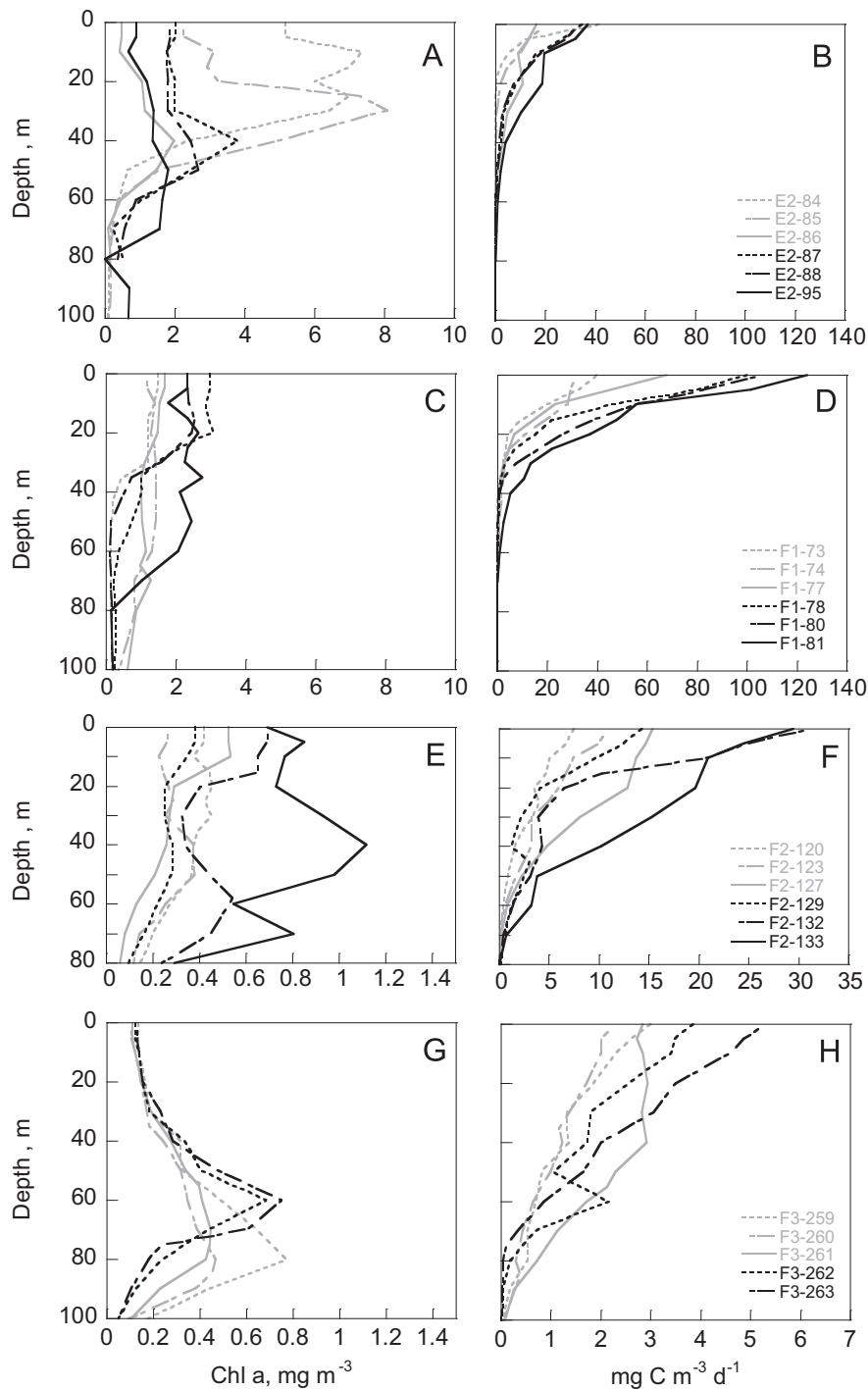


**Fig. 7.** Vertical distributions of Chl *a* concentration (A, C, E, G) and estimated *in situ* primary production (B, D, F, H) during F1, (A, B), E2 (C, D), selected stations of F2 (E, F) and F3 (G, H).

substantial between- and within-cruise scatter (data can be found in Table 3), in particular regarding E2.

The phytoplankton (nano-micro size range) community of the first two stations of F1 (Fig. 8A, C) was dominated by dinoflagellates and prymnesiophytes, including *Phaeocystis* sp. (with healthy-looking and senescent colonies) and coccolithophores like *Emiliania huxleyi*, *Calcidiscus leptoporus* and *Helicosphaera carteri*, but the higher salinities and Chl *a* concentrations of the last stations were associated to a stronger contribution of diatoms like *Chaetoceros* spp. and *Pseudo-nitzschia* spp., accompanied by *Lauderia annulata* and *Dytilum brightwellii*, among others. During E2 (Fig. 8B, D), the phytoplankton consisted of diatom taxa like *Chaetoceros* spp. (with the presence of

spores at all stations), *Pseudo-nitzschia* spp. and *Thalassiosira* spp., with a substantial contribution of dinoflagellates (mostly small gymnodinioids), and haptophytes (including colonial *Phaeocystis*, flagellate forms and coccolithophores). HPLC analyses confirmed these findings and revealed also the presence of prasinophytes, pelagophytes and cryptophytes (Gutiérrez-Rodríguez et al., 2010). The dominance of diatoms was particularly important at stations E2-84, E2-85 and E2-87 (Fig. 8B, D), while the contribution of *Phaeocystis* sp. and other haptophytes increased at the last two stations (E2-88 and E2-95). The phytoplankton community of F2 (Fig. 8E, G) was characterized by the scarcity of diatoms, the dominance of dinoflagellates and again the occurrence of both, healthy-looking and senescent colonies of

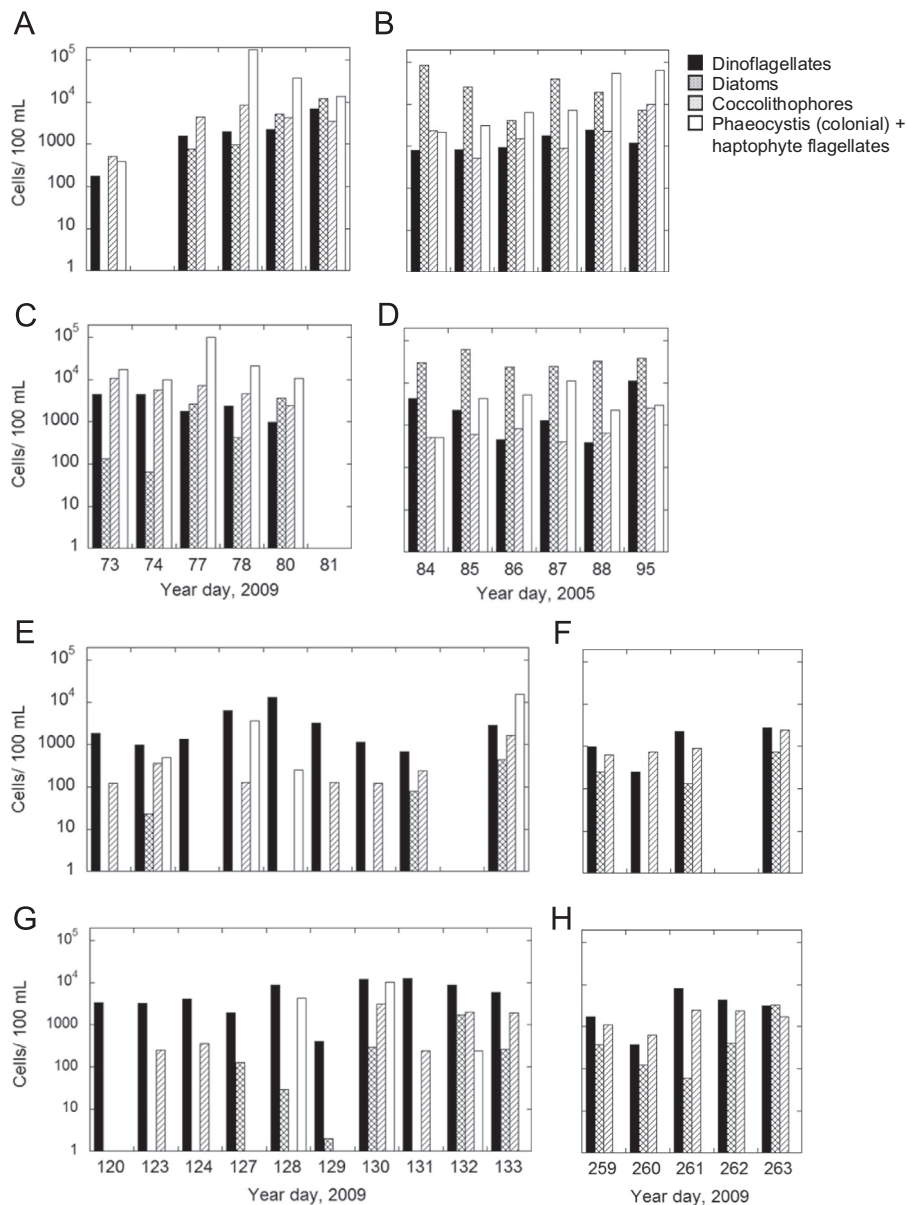


**Fig. 8.** Abundance of major phytoplankton groups (in cells/100 mL) in surface (A, B, E, F) and DCM (C, D, G, H) samples. Cruises F1 (A, C), E2 (B, D), F2 (E, G) and F3 (F, H).

*Phaeocystis* sp., in the latter case with the associated presence of numerous cryptophyte-looking heterotrophic flagellates (reaching concentrations of nearly 400 cells  $\text{mL}^{-1}$ ) that appeared to be feeding on the colonies. During the stratification phase (F3, Fig. 8F, H), the phytoplankton community was dominated by dinoflagellates, but the diversity of coccolithophores was higher than in the previous cruise. However, diatoms, represented mainly by small *Chaetoceros* spp. could be relatively abundant at some stations. The picophytoplankton of the FAMOSO surveys (Gomes et al., under review) was dominated by *Synechococcus* in F1 and F2, with an important contribution of picoeukaryotes in F1. *Prochlorococcus* was not detected in F2 but was present in F1 and, in F3, was more abundant than *Synechococcus* below 25 m.

### 3.2. Photosynthesis-irradiance (*P-E*) relationships

The values of  $P_m^B$  ranged from 0.327  $\text{mg C (mg Chl } a)^{-1} \text{ h}^{-1}$  for the DCM sample of F3-259 to 5.89  $\text{mg C (mg Chl } a)^{-1} \text{ h}^{-1}$  for the 5 m one of F1-81 (Table 3).  $P_m^B$  could not be calculated for station E2-84 because C uptake showed a lineal relationship with PAR

throughout the whole irradiance range used for the *P-E* curve. For E2-85, on the following day,  $P_m^B$  presented the lowest values of the cruise, both for the 5 m [ $1.18 \text{ mg C (mg Chl } a)^{-1} \text{ h}^{-1}$ ] and the subsurface samples [ $0.540 \text{ mg C (mg Chl } a)^{-1} \text{ h}^{-1}$ ]. The mean values (Table 3) of  $P_m^B$  at surface [ $3.29\text{--}3.98 \text{ mg C (mg Chl } a)^{-1} \text{ h}^{-1}$ ] were not significantly different between cruises (Kruskal–Wallis test). At each station,  $P_m^B$  at the DCM depth was generally lower than at surface, although the difference was only significant for E2 and F3 (Wilcoxon test,  $p < 0.05$ ).

At surface, the initial slope of the *P-E* curve,  $\alpha^B$  (Table 3), ranged from 0.002 to 0.015  $\text{mg C (mg Chl } a)^{-1} (\mu\text{mol photons } \text{m}^{-2} \text{ s}^{-1})^{-1} \text{ h}^{-1}$  in winter-spring (E2, F1 and F2) and from 0.015 to 0.020  $\text{mg C (mg Chl } a)^{-1} (\mu\text{mol photons } \text{m}^{-2} \text{ s}^{-1})^{-1} \text{ h}^{-1}$  in late summer (F3). Mean surface values ( $\pm$ SD) ranged from  $0.006 \pm 0.004 \text{ mg C (mg Chl } a)^{-1} (\mu\text{mol photons } \text{m}^{-2} \text{ s}^{-1})^{-1} \text{ h}^{-1}$  during E2 to  $0.016 \pm 0.004 \text{ mg C (mg Chl } a)^{-1} (\mu\text{mol photons } \text{m}^{-2} \text{ s}^{-1})^{-1} \text{ h}^{-1}$  during F3.  $\alpha^B$  values for the DCM samples were similar to those at surface for the winter cruises, and higher in spring and late summer; however, the difference was only significant for F2 (Wilcoxon test,  $p < 0.01$ ). Substantial

photoinhibition was only observed for the deep samples of September 2009. Excluding DCM samples from E2, which formed a separate cluster, optical depth (Fig. 9) was positively correlated ( $r=0.52$ ,  $p<0.001$ ,  $n=22$ ) with  $\alpha^B$  and negatively with  $E_k$  ( $r=-0.57$ ,  $p<0.001$ ,  $n=21$ , after omitting an outlier corresponding to station E2-88, with  $E_k=1400$ ). There was no correlation between  $\alpha^B$  and  $P_m^B$ , either for the whole data set or for each cruise.

### 3.3. Carbon fixation in 24 h on-deck incubations. Comparison with P-E-derived estimates

For the highest incubation irradiances (39.81–50%), the daily C fixation rates of the 5 m sample estimated from the 24 h  $^{14}\text{C}$  incubation experiments carried out on deck and from the 2 h P-E curve were well correlated ( $r=0.97$ ,  $0<0.001$ ,  $n=15$ ) (Fig. 10A). The major axis regression slope was 0.86 (0.73–1.0, 95% confidence limits). However, when the whole range of experimental light levels was considered (spanning from 0 to 39.81–50% of incident light), the relationship between the Chl *a*-normalized daily C fixation rates from 24 h and P-E incubations for equivalent light intensity conditions showed a convex shape (Fig. 10B–D). C fixation rates in 24 h incubations remained relatively stable and higher than P-E-derived values from intermediate light levels down to 4–18% in F1 and F2, and to 20–30% in F3 (Fig. 10B–D).

### 3.4. Primary production and phytoplankton biomass

P-E-derived estimates of daily primary production in the water column peaked at the surface in all the cruises, but presented high variability, both between and within cruises. C fixation rates at surface ranged between  $124\text{ mg C m}^{-3}\text{ d}^{-1}$  at the weakly stratified station F1-81 on 22 March 2009, to  $2.3\text{ mg C m}^{-3}\text{ d}^{-1}$  at the

strongly stratified station F3-260 on 17 September 2009 (Fig. 7B, D, F, and H). In F3, the percentage of primary production occurring below 50 m was between 11 and 28% of the total integrated value down to 80 m depth.  $\text{PP}_{\text{int}}$  ranged from a maximum close to  $2000\text{ mg C m}^{-2}\text{ d}^{-1}$  in March 2009 (station F1-81) to less than  $100\text{ mg C m}^{-2}\text{ d}^{-1}$  in September 2009. Cruise averages (Table 3) went from  $1024\text{ mg C m}^{-2}\text{ d}^{-1}$  in F1 to  $141\text{ mg C m}^{-2}\text{ d}^{-1}$  in F3, with intermediate values for E2 ( $417\text{ mg C m}^{-2}\text{ d}^{-1}$ ) and F2 ( $448\text{ mg C m}^{-2}\text{ d}^{-1}$ ). There was a significant linear relationship between  $\text{PP}_{\text{int}}$  and surface Chl *a* (Chl  $a_s$ ) or integrated Chl *a* (Chl  $a_{\text{int}}$ ) when the E2 data were excluded (Fig. 11A, B). However, the highest  $\text{PP}_{\text{int}}$  values, found during F1 (late March of 2009), did not coincide with the highest surface and integrated Chl *a* concentrations, which were measured in E2 (mid-March of 2005).

### 3.5. Relationships between primary production and physico-chemical forcing

When the whole data set was considered,  $\text{PP}_{\text{int}}$  decreased with increasing vertical stratification index (VSI) from winter to late summer, but the relationship could be negative (F1), positive (E2 and F2) or non-existent (F3) for the individual cruises (Fig. 12A). The  $\text{PP}_{\text{int}}$  to Chl *a* ratio ( $\text{PP}_{\text{int}}:\text{Chl } a_{\text{int}}$ ) was not correlated with total incident irradiance for values of this variable above approximately  $35\text{ mol photons m}^{-2}\text{ d}^{-1}$ , which included the samples from F1 and F2. However, the correlation between  $\text{PP}_{\text{int}}:\text{Chl } a_{\text{int}}$  and surface incident irradiance was significantly positive during the cruises E2 and F3 (Fig. 12B), for which incident irradiance was generally lower than the  $35\text{ mol photons m}^{-2}\text{ d}^{-1}$  threshold (Fig. 12B).  $\text{PP}_{\text{int}}$  and surface incident irradiance were significantly correlated only for F3 ( $r=0.91$ ,  $p<0.01$ ,  $n=5$ ; data not shown).

Cruise-averaged DIN and DIP fluxes to the euphotic layer declined strongly, due to the reduction of the diffusion coefficients through the

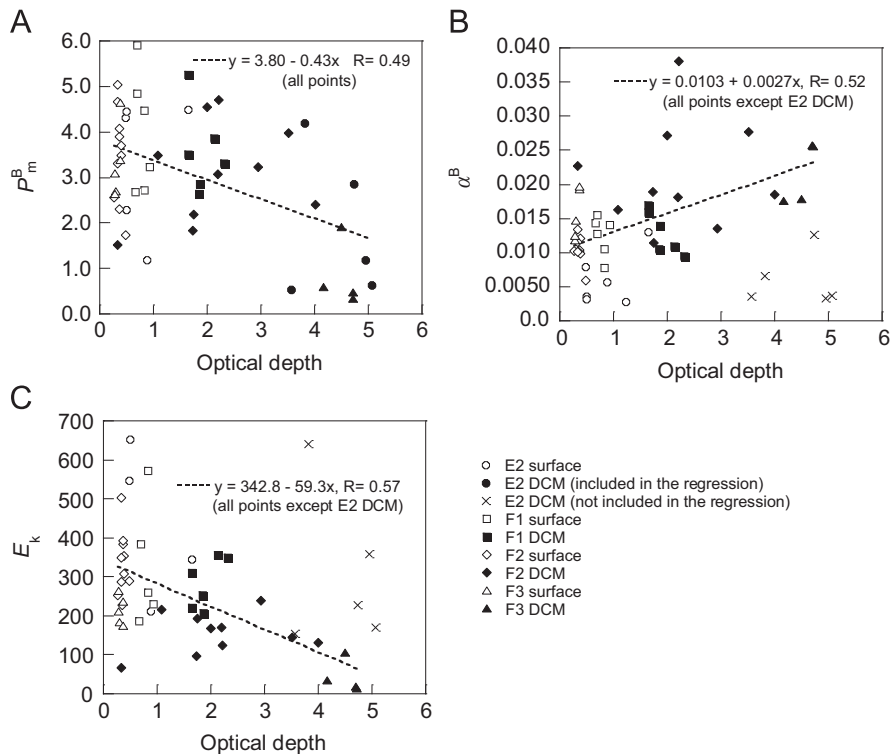


**Fig. 9.** Relationships between optical depth and (A)  $P_m^B$ , [ $\text{mg C}(\text{mg Chl } a)^{-1}\text{ h}^{-1}$ ], (B)  $\alpha^B$  [ $\text{mg C}(\text{mg Chl } a)^{-1}(\mu\text{mol photons m}^{-2}\text{ s}^{-1})^{-1}\text{ h}^{-1}$ ] and (C)  $E_k$  ( $\mu\text{mol photons m}^{-2}\text{ s}^{-1}$ ). Dashed lines are regression lines for (A) all points, (B) all points except the E2 DCM samples (the DCM point of station E2-84 is not shown) and (C), all points except the deep samples from E2 and the surface sample from station E2-88 (all correlations are significant, with  $p<0.05$ ). The symbols used for E2 DCM are different in A and the other graphs, to highlight that these points have not been included in the regressions shown in B and C.

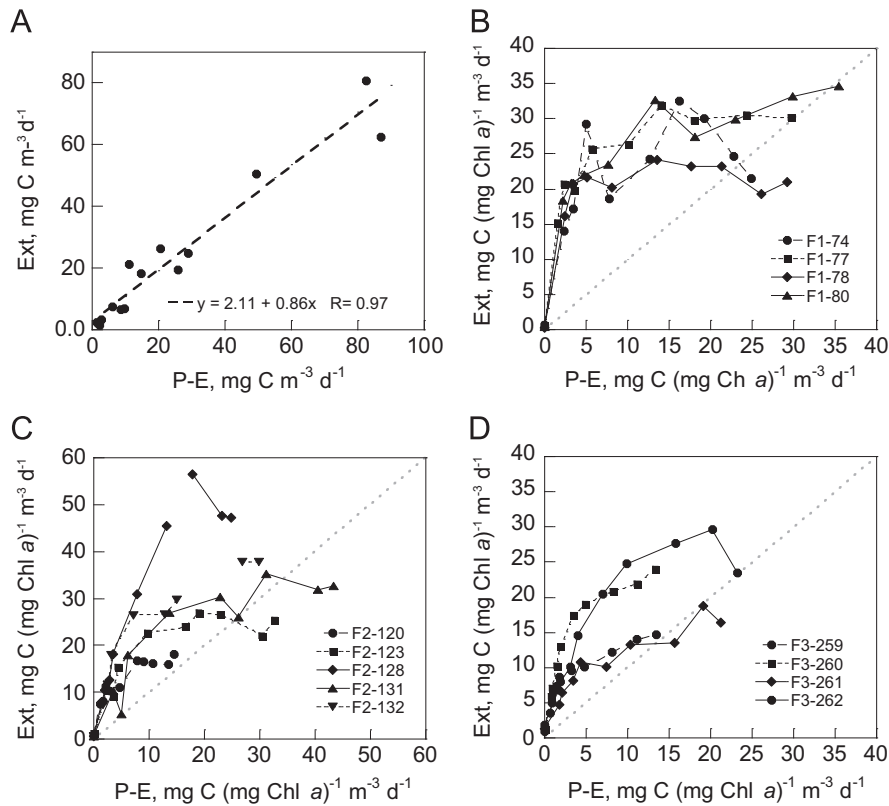


**Fig. 10.** Relationships between C fixation rates obtained from on-deck, 24 h incubations (Ext), and derived from the  $P-E$  curves ( $P-E$ ). (A) Relationship between the daily C fixation rates corresponding to the highest irradiances (39.81–50%) used in the on-deck incubations, and the corresponding C fixation rates in the  $P-E$  experiments; the dashed line is the major axis regression line. (B–D) Relationship between Chl  $a$ -normalized daily C fixation rates for different stations (indicated in the legend) of cruises F1 (B), F2 (C) and F3 (D); the gray dotted line indicates the relationship 1:1.

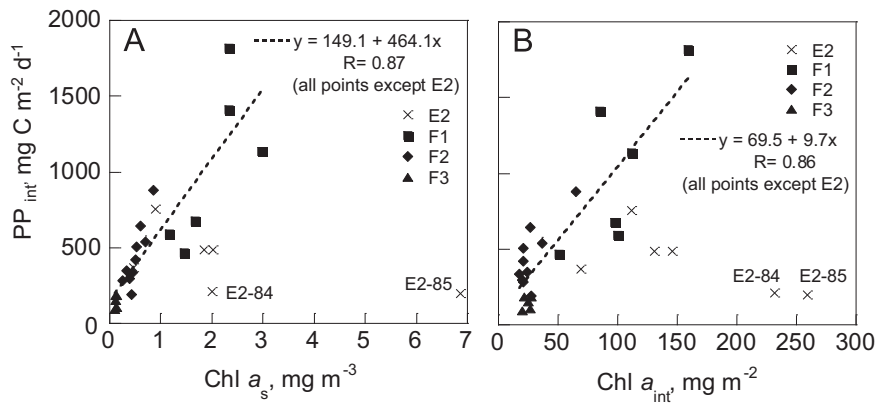


**Fig. 11.** Relationships between (A) surface (5 m) Chl  $a$  (Chl  $a_s$ ) and integrated primary production ( $PP_{int}$ ), (B) integrated Chl  $a$  (Chl  $a_{int}$ ) and  $PP_{int}$ .

thermocline, from a mean ( $\pm$ SD) of  $23.13 \pm 34.77 \text{ mmol m}^{-2} \text{ d}^{-1}$  for DIN and  $1.40 \pm 2.68 \text{ mmol m}^{-2} \text{ d}^{-1}$  for DIP in F1, to respective values of  $0.385 \pm 0.190 \text{ mmol m}^{-2} \text{ d}^{-1}$  and  $0.016 \pm 0.011 \text{ mmol m}^{-2} \text{ d}^{-1}$  in F2, and  $0.089 \pm 0.088 \text{ mmol m}^{-2} \text{ d}^{-1}$  and  $0.003 \pm 0.004 \text{ mmol m}^{-2} \text{ d}^{-1}$  in F3. There was a globally significant positive correlation between the logarithm of the upward DIN and DIP fluxes across the nutricline and the logarithm of  $PP_{int}$  (Fig. 12C, D). However, these relationships were not significant within cruises. As expected, the logarithms of the DIN and DIP fluxes of the whole data set were significantly correlated between themselves and with the logarithm of VSI (data not shown). The ratio between DIN and DIP fluxes was lower than the classical Redfield value of 16 only at stations F1-73, F1-74 and F2-132, while it ranged from 18 (F2-123) to 110 (F2-129) in the rest. The C equivalents

(according to the classic C, N, P Redfield ratios of 106, 16, 1) of the DIN and DIP upward fluxes were in general lower than the measured  $PP_{int}$  (the exceptions were stations F1-74 and F1-81 for DIN and station F1-74 for DIP). The molar ratios between  $PP_{int}$  and the C equivalents derived from the DIN fluxes were (mean  $\pm$ SD)  $2.9 \pm 2.2$ ,  $18.6 \pm 13.8$  and  $28.0 \pm 17.8$  for F1, F2 and F3, respectively. The corresponding values for DIP were  $5.7 \pm 6.2$ ,  $32.7 \pm 27.1$  and  $73.8 \pm 60.3$ .

The relationships among the within-cruise coefficients of variation of  $PP_{int}$  calculated with the “original” daily incident irradiance corresponding to each station (52%, 50%, 46% and 30%, respectively for F1, E2, F2 and F3) and with the same “sunny-day” incident irradiance for all the stations (54%, 29%, 48% and 11%, respectively), indicate that changes in incident irradiance played a

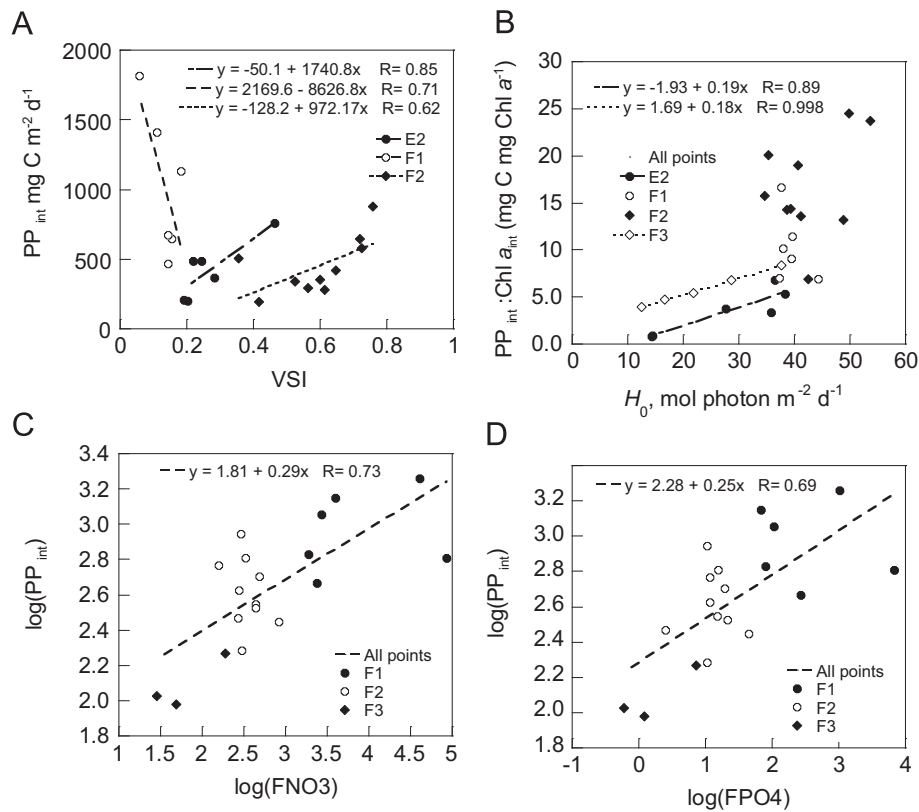


**Fig. 12.** Relationships between integrated primary production ( $PP_{int}$ ) and the integrated production to integrated biomass ratio ( $PP_{int}:\text{Chl } a_{int}$ ) with environmental variables. (A) relationship between  $PP_{int}$  and the vertical stratification index (VSI), (B) relationship between  $PP_{int}:\text{Chl } a_{int}$  and surface incident irradiance ( $H_0$ ), (C) log-log relationship between  $PP_{int}$ , and the flux of DIN (FNO<sub>3</sub>,  $\mu\text{mol m}^{-2} \text{d}^{-1}$ ), (D), log-log relationship between  $PP_{int}$ , and the flux of DIP (FPO<sub>4</sub>,  $\mu\text{mol m}^{-2} \text{d}^{-1}$ ).

minor role in F1 and F2, accounted for about 42% of the  $PP_{int}$  variability in E2 (mostly due to the effect of the low incident irradiances in E-84 and E-85) and for about 63% of it in F3.

During winter, hydrographic heterogeneity at the sampling point was important, as suggested by the remote sensing images (Fig. 4). The salinity increase, the deepening of the mixed layer (down to more than 200 m, Table 3) and the decrease of vertical stratification at the end of F1 (stations F1-80 and F1-81 on year days 80–81, Fig. 2) were accompanied by a three to four-fold rise of  $PP_{int}$ . This increase was a consequence of increments in both phytoplankton biomass and surface  $P_m^B$  (Table 3), a parameter which showed a significant positive correlation with surface salinity ( $r^2=0.94$ ,  $p<0.001$ ; data not shown). In this context, salinity could be considered as a proxy of the intensity of previous water column mixing (stronger mixing originates higher salinity in the upper layers). However, the relatively high salinities of the two first stations in E2, which had unusually high Chl  $a$  concentration (Fig. 3), were associated with shallow mixed layers. A connection between hydrographical and biological variability could also be made for the last three stations of F2, in which the Chl  $a$  and  $PP_{int}$  increases (Fig. 7E, F) were linked to a shallowing of the mixed layer and an increment of stratification (Tables 1 and 3).

## 4. Discussion

### 4.1. Hydrography and phytoplankton

The marked stratification increase between winter and late summer and the hydrographical characteristics of the cruises studied here are typical of the seasonal variation in the NW Mediterranean. In addition, the physico-chemical variables showed

substantial short-term variability, as can be seen in Figs. 2–6. In F1 and E2, the variability shown in the mesoscale heterogeneity of the surface fields (Fig. 4) and the interleaving of high and low salinity waters in the upper layer waters (Figs. 2 and 3) may be a result of the combination of several processes, including baroclinic instabilities associated with deep water formation, various restratification mechanisms and destratification events due to wind bursts (Lévy et al., 1999, 2000; Madec et al., 1991). During F2, the relatively high and homogeneous salinity of the upper water layer after day 128 (Fig. 5, Table 1) might reflect the crossing of a hydrographic structure comparable to the cyclonic eddy reported by Salat et al. (2013) based on satellite imagery.

The relatively high nutrient concentrations in the winter cruises are the result of deep convection and mixing, which are a characteristic of the study area (Siokou-Frangou et al., 2010) and were particularly intense in the cold and windy winters of 2004–2005 (Salat et al., 2007) and 2008–2009 (Salat et al., 2010). DIN concentrations at surface continued to be relatively high ( $>1 \text{ mmol m}^{-3}$ ) through spring (F2) and also exceeded  $1 \text{ mmol m}^{-3}$  in the late summer cruise (F3). This is a rather high value for this time of the year, as compared with the DYFAMED data (Marty et al., 2002), but we lack sufficient additional information to provide an explanation. The surface concentration of DIP only reached  $0.1 \text{ mmol m}^{-3}$  in the early March cruise (F1); in the others, surface DIP concentrations did not exceed  $0.05 \text{ mmol m}^{-3}$ .

The winter cruises, F1 and E2, present a well-developed diatom-dominated phytoplankton bloom. In these cruises, the dynamism and patterns of variability of the Chl  $a$  (Fig. 4B–E) reflect a strong hydrodynamic signal, which can be associated to meanders and eddies of the untransformed Atlantic Waters recently penetrated from the South, and the Liguro-Provençal-Catalan Current flowing from the NW to the SE (Fig. 4A). The

highest surface and integrated Chl *a* values recorded in our study were measured in March, in agreement with *in situ* measurements at the DYFAMED station (43° 25'N, 07° 52'E), situated in the central Ligurian Sea (Marty and Chiavérini, 2002), and satellite-based reports that locate the Chl *a* peak of the NW Mediterranean in late winter–early spring (Bosc et al., 2004; D'Ortenzio and Ribera d'Alcalà, 2009). During E2, Chl *a* concentrations at 5 m depth reached 7 mg m<sup>-3</sup> at station E2-84, on 25 March 2005 (Table 3). This is one of the highest values measured in the open sea region (seawards of the shelf slope) of the NW Mediterranean, where Chl *a* concentrations beyond 3 mg m<sup>-3</sup> have rarely been reported (Siokou-Frangou et al., 2010). The high Chl *a* concentration found in March 2005 is probably related to the unusually cold 2004–2005 winter, in which the convection process that produces the Western Mediterranean Deep Water was particularly intense and affected not only the Gulf of Lion area, but also the Catalan and the western Ligurian sub-basins (Salat et al., 2007; Smith et al., 2008). This intense deep convection event induced an extraordinary nutrient enrichment of the surface waters and subsequent phytoplankton biomass build-up in the NW Mediterranean region (Volpe et al., 2012; Arin et al., 2013). On 25 March 2005, the integrated Chl *a* concentration reached 260 mg m<sup>-2</sup>, a value similar to the maxima (230 and 250 mg C m<sup>-2</sup>) registered by Marty and Chiavérini (2002) and by Morán and Estrada (2005), respectively.

The composition of the nano-microphytoplankton communities during the E2 and FAMOSO cruises followed a typical seasonal pattern for the region (Siokou-Frangou et al., 2010, Estrada and Vaqué, 2013). F1 and E2 appeared to present, respectively, an early and a late winter-spring bloom situation with strong contributions of the diatoms *Chaetoceros* spp., *Pseudonitzschia* spp. and *Thalassiosira* spp., and the haptophyte *Phaeocystis* sp. During F2 (post-bloom) and F3 (late summer conditions), the phytoplankton was dominated by dinoflagellates and coccolithophores. It must be noted that, although a diatom-dominated winter-spring bloom has been documented in coastal zones throughout the Mediterranean, the occurrence of diatom proliferations in the open sea seems to be limited to areas where processes like deep convection, fronts or gyres sufficiently enrich the surface waters (Siokou-Frangou et al., 2010). *Phaeocystis* sp. is an important contributor to the winter-spring blooms in the NW Mediterranean and may be the dominant taxon in regions where diatoms do not proliferate (Estrada, 1991). Its higher abundances appear to be associated with Recent Atlantic Waters of relatively low salinity. For example, in March 1985, high Chl *a* concentrations offshore of the Catalan Front were due to a proliferation of *Phaeocystis* sp. (Estrada, 1991) and, in February–March 1999, an anticyclonic eddy of Recent Atlantic Waters at the northern boundary of the Balearic Sea (Pascual et al., 2002) was characterized by a community of *Phaeocystis* and other haptophytes (Estrada et al., 2003). The association of *Phaeocystis* sp. with Recent Atlantic Waters would explain the opposite population density changes of diatoms (increasing) and *Phaeocystis* sp. + haptophyte flagellates (decreasing) with increasing salinity in the last three stations of F1 and E2 (Figs. 2B, 3B, 9A and B).

#### 4.2. Photosynthetic parameters

The average values of March surface Chl *a*-normalized maximum photosynthetic rates,  $P_m^B$ , (Table 3) were somewhat higher than those reported by Morán and Estrada (2005) for March 1999 [mean ± SD, 2.32 ± 0.76 mg C (mg Chl *a*)<sup>-1</sup> h<sup>-1</sup>],  $P_m^B$  (mean ± SD) increased slightly from winter [3.34 ± 1.42 mg C (mg Chl *a*)<sup>-1</sup> h<sup>-1</sup> for E2 and 3.98 ± 1.32 mg C (mg Chl *a*)<sup>-1</sup> h<sup>-1</sup> for F1] to spring [3.47 ± 1.04 mg C (mg Chl *a*)<sup>-1</sup> h<sup>-1</sup>], to remain within the same range through late summer [3.29 ± 0.82 mg C (mg Chl *a*)<sup>-1</sup> h<sup>-1</sup>], a

pattern that agrees with the findings of Morán and Estrada (2005) and Marty and Chiavérini (2002). Assuming a  $Q_{10}$  value of 1.88 (Eppley, 1972, Bissinger et al., 2008), the variation of temperature between winter and late summer (13–24 °C) should theoretically double  $P_m^B$ . However, the between-cruise differences in the  $P_m^B$  averages are smaller than two-fold, indicating that other factors, such as irradiance conditions, nutrient availability, and phytoplankton composition and physiological state override temperature effects. Significant differences between  $P_m^B$  in surface and DCM of the same station could be found even in relatively well-mixed winter waters (E2), indicating that the time scale for photoacclimation was faster than for mixing. In contrast to  $P_m^B$ , surface and DCM  $\alpha^B$  were practically the same at all stations of the two winter cruises, suggesting a slower response of this parameter (Morán and Estrada, 2005). When all the data were considered, the lowest  $P_m^B$  corresponded to optical depths (OD) > 3 (Fig. 9A). This observation and the overall positive correlation of  $\alpha^B$  (and negative of  $E_k$ ) with OD (Fig. 9) (the exception were the deep samples from E2) agree with previous work associating  $\alpha^B$  increase (and  $P_m^B$  and  $E_k$  decrease) with photoacclimation to lower irradiances (Falkowski, 1981; Moore et al., 2006). There was no relationship between  $P_m^B$  and MLD (data not shown), suggesting that phytoplankton communities had at least partially photoacclimated to *in situ* irradiance. In this sense, stations F1-80 and F1-81 with MLDs exceeding 200 m, and hence with phytoplankton communities presumably exposed to low average light levels, presented  $P_m^B$  values that were among the highest of our data set (Tables 1 and 3). The coexistence of high  $P_m^B$  (and  $E_k$ ) with deep MLDs at these stations agrees with the results of Moore et al. (2006), who found that populations of mixed water columns were acclimated to relatively high irradiances, and proposed that this response could represent a strategy to avoid excessive photoinhibition damage. In contrast to the high  $P_m^B$  of the last stations of F1, it was not possible to define a saturated C fixation rate for the *P-E* curves of station E2-84, carried out about the same time of the year (but in 2005), while the  $P_m^B$  for both surface and 20 m deep samples of the next day station, E2-85, were among the lowest recorded in this study. Physiological parameters derived from fast repetition rate fluorometer (FRRF) measurements in these stations were coherent with these peculiar characteristics of their phytoplankton communities (Gutiérrez-Rodríguez, unpublished results). Thus, a maximum of *in situ* electron transport rates ( $ETR_{max}$ ) could not be assessed for E2-84 while the  $ETR_{max}$  attained in surface waters of E2-85 was again among the lowest values recorded in this data set (data not shown). Moreover, the corresponding  $\alpha^B$  and  $E_k$  values (Table 3) were also outliers in the overall relationship between these parameters and OD (Fig. 9). E2-84, E2-85 and in general all E2 stations presented a diatom-dominated phytoplankton community with substantial presence of *Chaetoceros* spores, suggesting that the bloom was in a decay phase. Given the high phytoplankton biomass accumulated at E2-84, E2-85 and although to a lower degree at other E2 stations, it seems feasible that rapidly growing diatoms had consumed a large portion of the available nutrients, leading to nutrient starvation. This view is supported by FRRF observations during E2, which showed a marked decrease of Photosystem II maximum quantum yield ( $F_v/F_m$ ) and an increase of effective absorption cross-section (sPSII) in the upper part of the water column, both during the day and at night (Gutiérrez-Rodríguez, unpublished results). As there were no substantial changes in the phytoplankton community composition of the surface and deep samples of E2, an observation that is consistent with the relatively well-mixed water column, these vertical patterns of  $F_v/F_m$  and sPSII can be taken as an indicator of nutrient starvation and unbalanced growth (Parkhill et al., 2001; Suggett et al., 2009). However, narrow MLDs (26–22 m) and high vertical attenuation with shallow euphotic layers (19–26 m) at

both E-84 and E-85, which coincided with surface incident irradiance about half that of the following days (Tables 1 and 3) due to covered skies, suggest that light-limitation could also contribute to the distinctive photosynthetic parameters assessed at these stations. The above examples indicate that different photoacclimation strategies may be very important in determining phytoplankton growth in oligotrophic ecosystems and must be taken into account in model parameterizations (Ayata et al., 2013), emphasizing the need for *in situ* measurements.

#### 4.3. Comparison between *P-E* curves and on-deck incubations

As can be seen in Fig. 10A, for the highest incubation irradiance the relationship between daily C fixation rates derived from *P-E* experiments and from on-deck incubations is linear. However, when Chl *a*-normalized daily C fixation values for the whole range of incubation irradiances are considered (Fig. 10B–D), the relationship between measurements from *P-E* experiments and from 24 h on-deck incubations presents generally higher values for the external than for the *P-E* incubations and tends to be more convex in F1 and F2 than in F3. It must be noted that light attenuation was obtained with blue filters in the on-deck incubators and with neutral (levels of gray) screens in the *P-E* ones. However, the observation that stations with less convex curves were the most stratified of the data set (F3) suggest that the differences between incubation methods could be related to a photoacclimation response to the experimental intensity (rather than quality) of light exposure. In fact, photoacclimation was evidenced by flow cytometrically detected changes in fluorescence per cell in 24 h dilution experiments carried out during E2 (Gutiérrez-Rodríguez et al., 2010). The bias introduced by photoacclimation into estimates of  $PP_{int}$  is generally limited by the fact that the highest contribution to  $PP_{int}$  comes generally from the well illuminated upper part of the water column, for which the differences between incubation systems due to photoacclimation tend to be relatively small (Fig. 10A). To make a rough comparison, a daily integrated primary production for a water column layer between surface and the DCM was calculated using the light transmission data in combination with either the *P-E* parameters ( $PP_{s,int,PE}$ ) or the C fixation rates derived from the external incubator ( $PP_{s,int,Ext}$ ). The average ratio ( $\pm$  SD) between the corresponding values of  $PP_{s,int,PE}$  and  $PP_{s,int,Ext}$  (15 data pairs, data not shown) was  $0.99 \pm 0.41$ . The slope of the major axis regression line between these variables was not significantly different from 1 for a 0.99 confidence interval ( $PP_{s,int,Ext} = 1.12 PP_{s,int,PE} - 38.33$ ,  $r = 0.85$ ,  $n = 15$ ). Although this result indicates that  $PP_{int}$  estimates may vary little for the incubation techniques compared here, it can be concluded that, for static incubations, shorter incubation times should be preferable if photoacclimation changes are to be avoided. In the following sections, reference will be made only to the primary production results derived from the *P-E* curves.

#### 4.4. Relationships between environmental variables, phytoplankton biomass and primary production

There was a clear seasonal variability of  $PP_{int}$ , which went from  $95 \text{ mg C m}^{-2} \text{ d}^{-1}$  on 17 September 2009 to  $1800 \text{ mg C m}^{-2} \text{ d}^{-1}$  on 22 March 2009 (Table 3). The range of  $PP_{int}$  found during our study agreed with that reported by Marty and Chiavérini (2002) for the time series of the DYFAMED station. A similar maximum  $PP_{int}$  value ( $1700 \text{ mg C m}^{-2} \text{ d}^{-1}$ ) was recorded by Morán and Estrada (2005) for a station occupied during March 1999 in the shelf slope front, to the west (around  $3^\circ \text{ E}$ ) of our study area. Measurements obtained during E2 were in general an exception to the good relationships between Chl  $a_c$  and Chl  $a_{int}$  with  $PP_{int}$  (Fig. 11A, B). In this cruise, the high ratio between integrated and

surface Chl *a* corresponding to station E2-85 (Table 3) appears to reflect the subduction of the Chl *a*-rich water body found at E2-84 (Fig. 3) under a Chl *a*-poorer surface layer of lower salinity waters. On the other hand, both E2-84 and E2-85 presented relatively low  $PP_{int}$  values (Fig. 11A, B). A similar situation was found in DYFAMED (Marty and Chiavérini, 2002), where the highest Chl *a* concentrations ( $230 \text{ mg m}^{-2}$  in March 1999) were associated to relatively low  $PP_{int}$  ( $307 \text{ mg C m}^{-2} \text{ d}^{-1}$ ). As noted in Section 4.2, FRRF measurements and other observations such as the presence of *Chaetoceros* spores suggest that the phytoplankton of stations E2-84 and E2-85 was undergoing some physiological stress and entering a stage of decay.

Only E2 and F3 showed significant positive relationships between  $PP_{int}:\text{Chl } a_{int}$  and incident irradiance at the surface water. These two cruises presented surface irradiances generally below  $35 \text{ mol photons m}^{-2} \text{ d}^{-1}$ , which appeared to indicate a threshold for light limitation of  $PP_{int}$  (Fig. 12B). This finding supports the conclusion of Morán and Estrada (2005), who found that the  $PP_{int}:\text{Chl } a_{int}$  ratios at NW Mediterranean stations sampled during March 1999 and January–February 2000 were positively related to incident irradiances ranging between  $10 \text{ mol photons m}^{-2} \text{ d}^{-1}$  and  $38 \text{ mol photons m}^{-2} \text{ d}^{-1}$ .

Much of the between-cruise variability of  $PP_{int}$  appears to be controlled, directly or indirectly, by the stratification of the water column, as reflected in the overall relationships of  $PP_{int}$  with VSI and with the nutrient fluxes across the nutricline (Fig. 12A, C and D). As VSI increases from winter to late summer, the nutriclines and the Chl *a* maxima deepen, the diffusion coefficient and the nutrient fluxes across the nutricline decrease and  $PP_{int}$  becomes limited by nutrient exhaustion in the upper layers and low light at the nutricline level. Under these conditions, as found for F3, there is no correlation between  $PP_{int}$  and VSI (Tables 1–3, the data are not shown in Fig. 12A). In contrast, in the winter and spring cruises, the positive (E2, F2) or negative (F1) relationship between  $PP_{int}$  and VSI (Fig. 12A) could be linked to hydrographical heterogeneity of the water bodies and differences in the composition and history of the associated phytoplankton community and planktonic food web (see Section 4.1). The increase of the average ratio between  $PP_{int}$  and the C equivalent corresponding to the nutrient fluxes (Section 3.5) agrees with the general picture of an increasing contribution of nutrient recycling to phytoplankton growth expected under increasing stratification. However, neither nutrient concentrations in the euphotic zone nor nutrient fluxes across the nutricline showed any meaningful within-cruise relationships with  $PP_{int}$  or with the photosynthetic parameters. In addition to the methodological errors and limitations that affect the calculation of these variables, one should be aware that nutrient concentrations, nutrient fluxes across the nutricline and C fixation rates in short-term experiments are controlled by processes acting at different time scales. Phytoplankton cells integrate environmental and ecological (zooplankton grazing, for example) influences over variable periods of time, and C uptake in primary production experiments may be modulated by factors such as taxonomical affinity, optical history of the cells, nutrient fluxes across the cell membrane or internal nutrient quotas (Falkowski and Raven, 2007). These constraints make it difficult to relate environmental nutrient variables with the short-term physiological response of the cells. This difficulty is particularly important for fast-recycling nutrients such as phosphorus (Benitez-Nelson, Buesseler, 1999). Assuming half saturation constants of approximately  $0.5\text{--}1 \text{ mmol m}^{-3}$  (Laws, 2013), DIN concentrations, which were seldom lower than  $1 \text{ mmol m}^{-3}$  at surface (Section 3.1), could have been non-limiting in all the cruises. Given that there are reports of almost fully saturated growth rates for phosphate concentrations below the limit of detection of usual colorimetric techniques (Laws, 2013), phosphorus could have been non-limiting in F1, but the situation for the other cruises is

uncertain. There are no silicate data for the FAMOSO cruises; the mean concentration of this nutrient in E2 was lower than that of DIN. Assuming a half saturation concentrations around  $1 \text{ mmol m}^{-3}$  (Aumont et al. 2003), and considering the very scarce presence of diatoms in surface waters of the post-bloom phase (Fig. 8E), it is likely that silicate could have limited or co-limited diatom growth at the end of the bloom. In this context, there is a relevant distinction between nutrient limitation, which refers to balanced growth at a rate acclimated to nutrient supply, and nutrient starvation, which refers to unbalanced growth when cellular demand exceeds nutrient supply rate (Parkhill et al., 2001). As discussed below, it is likely that in situations of high biomass like those found in the first stations of E2, relatively low availability of DIN, DIP or both could have caused nutrient starvation.

Superimposed to the seasonal trends, the Chl *a* concentration and primary production measured during this study revealed a high day-to-day spatio-temporal variability, which was particularly important during the winter-spring bloom period and was only in a minor part associated to fluctuations in daily irradiance (see Section 3.5). The intricate satellite-based winter distributions of surface Chl *a* (Fig. 4) suggest an important role of hydrographical mesoscale and sub-mesoscale forcing in the short-term spatio-temporal fluctuations of phytoplankton standing stock and primary production. A detailed comparison of the stations within each of the winter cruises covering the phytoplankton bloom period may provide valuable insight on the links between environmental forcing and phytoplankton response. The particularities of some of the E2 samples have been discussed in Section 4.2 and in the first paragraph of this section. In the case of F1, the last two biological stations (F1-80 and F1-81, on 21 and 22 March 2009, respectively), which showed the highest  $\text{PP}_{\text{int}}$  values recorded in this study, presented upper mixed layers deeper than 200 m (Table 3). For comparison, Siegel et al. (2002) estimated a median critical depth of 181 m as characteristic of the initiation of the spring bloom at latitudes of 40–45° N in the North Atlantic. If all the CTD casts (including other stations in addition to the biological ones) performed between 21 and 22 March 2009 are considered, the MLD fluctuated from 115 m (a cast at 19:30 on 21 March) to the whole water column depth of approximately 2190 m (a cast at 20:26 GMT on 21 March 2009). In parallel with the increase in MLD, these last stations of F1 presented a decrease of the stratification index and an increment of  $\text{PP}_{\text{int}}$ . The coincidence, on 21 March 2009, of a water column mixed down to the bottom (2190 m) with high  $\text{PP}_{\text{int}}$  ( $1400 \text{ mg C m}^{-2} \text{ d}^{-1}$ ) and a concentration of  $2.33 \text{ mg m}^{-3}$  of Chl *a* at the surface, typical of a well-developed bloom situation, is intriguing. The MLD values reported here must be taken with caution, not only because of the subjectivity involved in their determination from CTD recordings (de Boyer Montégut et al., 2004), but also because homogeneous variable profiles do not represent evidence of active mixing at the time of sampling (Mouriño-Carballido, personal communication). However, the high variability of MLD determined during the last days of F1 and the agreement between the patterns of variability of hydrographical variables and *in vivo* fluorescence (Fig. 2) suggests that the changes in the vertical structure of the water column of these stations are due to mesoscale hydrographical forcing occurring after a phytoplankton bloom had already developed. As noted by Lévy et al. (1999, 2000) the winter-spring bloom in the NW Mediterranean is not a steady phenomenon but presents a high spatio-temporal variability from onset to decay. The close relationship between variation in salinity,  $P_m^B$  and phytoplankton composition at these last stations of F1 must be taken as a reflection of ecological history (including the interactions with the other components of the food web), not as a direct effect of hydrographical variables such as salinity. As mentioned in Section 3.5, high salinities indicate a stronger mixture with deep, nutrient-rich waters, and therefore, the capability to sustain the development of a high phytoplankton biomass based on fast-growing groups such as diatoms.

In summary, our findings underline the importance of the winter-spring phytoplankton bloom in the deep convection region of the NW Mediterranean as a contributor to phytoplankton biomass and primary production in the region. However, during the bloom period, both phytoplankton biomass and primary production showed considerable variability at the scale of days, in connection with the intense hydrographic mesoscale heterogeneity in the region and with the physiological and ecological history of the planktonic communities associated with each water body. The observation that the relationships between surface phytoplankton biomass and primary production could show substantial variability has implications for estimates of primary production based on remote sensing.

## Acknowledgments

This work was supported by the Spanish Projects EFLUBIO REN2002-04151-C02, FAMOSO (CTM2008-06261-C03) and TURBIMOC (CTM2009-06712-E/MAR), and partially by the Grup de Recerca of the (2009 SGR 588). B.F.-C. holds a FPU fellowship of the Spanish Government. We thank the crew and colleagues on board the R.V. “Cornide de Saavedra”, the R.V. “García del Cid” and the R.V. “Sarmiento de Gamboa” for their help during the cruises. Màxim Galindo contributed to the nutrient measurements and Paloma Chouciño collected microstructure turbulence observations. Remote sensing SST data were made available by Òscar Chic and the Coastal Ocean Observatory (<http://coo.icm.csic.es/>) at ICM-CSIC. We acknowledge the GES DAAC MODIS Data Support Team for making MODIS data available to the user community.

## References

- Arin, L., Guillén, J., Segura-Noguera, M., Estrada, M., 2013. Open sea hydrographic forcing of nutrient and phytoplankton dynamics in a Mediterranean coastal ecosystem. *Estuar., Coast. Shelf Sci.* 133, 116–128.
- Antoine, D., Morel, A., André, J., 1995. Algal pigment distribution and primary production in the eastern Mediterranean as derived from coastal zone color scanner observations. *J. Geophys. Res.* 100, 16193–16209.
- Aumont, O., Maier-Reimer, E., Blain, S., Monfray, P., 2003. An ecosystem model of the global ocean including Fe, Si, P colimitations. *Glob. Biogeochem. Cycles* 17 (2), 1060. <http://dx.doi.org/10.1029/2001GB001745>.
- Ayata, S.-D., Lévy, M., Aumont, O., Sciandra, A., Sainte-Marie, J., Tagliabue, A., Bernard, O., 2013. Phytoplankton growth formulation in marine ecosystems: should we take into account photo-acclimation and variable stoichiometry in oligotrophic areas? *J. Mar. Syst.* 125, 29–40.
- Benitez-Nelson, C.R., Buesseler, K.O., 1999. Variability of inorganic and organic phosphorus turnover rates in the coastal ocean. *Nature* 398, 502–505.
- Bissinger, J.E., Montagnes, D.J.S., Sharples, J., Atkinson, D., 2008. Predicting marine phytoplankton maximum growth rates from temperature: improving on the Eppley curve using quantile regression. *Limnol. Oceanogr.* 53, 487–493. <http://dx.doi.org/10.4319/lo.2008.53.2.0487>.
- Bosc, E., Bricaud, A., Antoine, D., 2004. Seasonal and interannual variability in algal biomass and primary production in the Mediterranean Sea, as derived from 4 years of SeaWiFS observations (GB1005). *Glob. Biogeochem. Cycles* 18, 1–17. <http://dx.doi.org/10.1029/2003GB002034>.
- de Boyer Montégut, C., Madec, G., Fischer, A.S., Lazar, A., Iudicone, D., 2004. Mixed layer depth over the global ocean: an examination of profile data and a profile-based climatology. *J. Geophys. Res.* 109, C12003. <http://dx.doi.org/10.1029/2004JC002378>.
- D’Ortenzio, F., Ribera d’Alcalà, M., 2009. On the trophic regimes of the Mediterranean Sea: a satellite analysis. *Biogeosciences* 6, 139–148.
- Eppley, R.V., 1972. Temperature and phytoplankton growth in the sea. *Fish. Bull.* 70, 1068–1085.
- Estrada, M., 1991. Phytoplankton assemblages across a NW Mediterranean front: changes from winter mixing to spring stratification. *Oecologia aquatica* 10, 157–185.
- Estrada, M., Morales-Blake, A., Arin, L., Blasco, D., Morán, X.A.G., Emiliano, M., 2003. The Winter Bloom in the Catalano-Balearic Sea (NW Mediterranean). Mesoscale Hydrographic Structures and the Distribution of Phytoplankton Assemblages. EGS-AGU-EUG Joint Assembly, Nice, France. Poster.
- Estrada, M., Vaqué, D., 2013. Microbial components. In: Goffredo, E., Dubinsky, Z. (Eds.), *The Mediterranean Sea: Its history and present challenges*. Springer, Dordrecht, pp. 87–111.

- Estrada, M., Varela, R.A., Salat, J., Cruzado, A., Arias, E., 1999. Spatio-temporal variability of the winter phytoplankton distribution across the Catalan and North Balearic fronts (NW Mediterranean). *J. Plankton Res.* 21, 1–20.
- Falkowski, P.G., 1981. Light–shade adaptation and assimilation numbers. *J. Plankton Res.* 3, 203–216.
- Falkowski, P.G., Raven, J.A., 2007. *Aquatic Photosynthesis*, 2nd ed. Princeton University Press, Princeton, New Jersey, USA p. 512.
- Falster, D.S., Warton, D.I., Wright, I.J., 2006. SMATR: Standardised Major Axis Tests and Routines, Ver 2.0. (<http://www.bio.mq.edu.au/ecology/SMATR/>).
- Gascard, J.-C., 1978. Mediterranean deep water formation, baroclinic instability and oceanic eddies. *Oceanol. Acta* 1 (3), 315–330.
- Gomes, A., Gasol, J.-M., Estrada, M., Franco-Vidal, L., Díaz-Pérez, L., Ferrera, I., Morán, X.A.G., 2014. Heterotrophic Bacterial Responses to the Winter–Spring Phytoplankton Bloom in Open Waters of the NW Mediterranean, under review.
- Grasshoff, K., Kremling, K., Ehrhardt, M. (Eds.), 1999. *Methods of Seawater Analysis*, 3rd ed. Verlag Chemie/Wiley-VCH, Weinheim/New York (600 pp.).
- Gutiérrez-Rodríguez, A., Latasa, M., Estrada, M., Vidal, M., Marrasé, C., 2010. Carbon fluxes through major phytoplankton groups during the spring bloom and post-bloom in the Northwestern Mediterranean Sea. *Deep-Sea Res. I* 57, 486–500.
- Isern-Fontanet, J., Hascoët, E., 2014. Diagnosis of high-resolution upper ocean dynamics from noisy sea surface temperatures. *J. Geophys. Res. Oceans* 119, 121–132. <http://dx.doi.org/10.1002/2013JC009176>.
- Jacques, G., Minas, H.J., Minas, M., Nival, P., 1973. Influence des conditions hivernales sur les productions phyto- et zooplanctoniques en Méditerranée Nord-Occidentale. II. Biomasse et production phytoplanktonique. *Mar. Biol.* 23, 351–365.
- Jacques, G., Minas, M., Neveux, J., Nival, P., Slawyk, G., 1976. Conditions estivales dans la divergence de Méditerranée nord-occidentale. *Phytoplankton. Ann. l'Inst. Océanogr.* 52, 141–152.
- Laws, E.A., 2013. Evaluation of *in situ* phytoplankton growth rates: a synthesis of data from varied approaches. *Annu. Rev. Mar. Sci.* 5, 248–268.
- Lévy, M., Mémery, L., Madec, G., 1998. The onset of a bloom after deep winter convection in the northwestern Mediterranean sea: mesoscale process study with a primitive equation model. *J. Mar. Syst.* 16, 7–21.
- Lévy, M., Mémery, L., Madec, G., 1999. The onset of the spring bloom in the MEDOC area: mesoscale spatial variability. *Deep-Sea Res. I* 46, 1137–1160.
- Lévy, M., Mémery, L., Madec, G., 2000. Combined effects of mesoscale processes and atmospheric high-frequency variability on the spring bloom in the MEDOC area. *Deep-Sea Res. I* 47, 27–53.
- Madec, G., Chartier, M., Delecluse, P., Crepon, M., 1991. A three-dimensional numerical study of deep water formation in the northwestern Mediterranean sea. *J. Phys. Oceanogr.* 21, 1349–1371.
- Marty, J.C., Chiavérini, J., 2002. Seasonal and interannual variations in phytoplankton production at DYFAMED time-series station, northwestern Mediterranean Sea. *Deep-Sea Res. II* 49, 2017–2030.
- Marty, J.C., Chiavérini, J., 2010. Hydrological changes in the Ligurian Sea (NW Mediterranean, DYFAMED site) during 1995–2007 and biogeochemical consequences. *Biogeosciences* 7, 2117–2128.
- Marty, J.C., Chiavérini, J., Pizay, M.D., Avril, B., 2002. Seasonal and interannual dynamics of nutrients and phytoplankton pigments in the western Mediterranean Sea at the DYFAMED time-series station (1991–1999). *Deep-Sea Res. II* 49, 1965–1985.
- Marty, J.C., Garcia, N., Raimbault, P., 2008. Phytoplankton dynamics and primary production under late summer conditions in the NW Mediterranean Sea. *Deep-sea Research I. Nature* 55, 1131–1149.
- MEDOC Group, 1970. Observation of formation of deep water in the Mediterranean Sea, 1969. *Nature* 227, 1037–1040.
- Moore, C.M., Suggest, D.J., Hickman, A.E., Kim, Y.N., Tweddle, J.F., Sharples, J., Geider, R.J., Holligan, P.M., 2006. Phytoplankton photoacclimation and photoadaptation in response to environmental gradients in a shelf sea. *Limnol. Oceanogr.* 51, 936–949.
- Morales, A., 2006. Estudio multitemporal de la clorofila superficial en el Mar Mediterráneo Noroccidental, evaluada a partir de datos SeaWiFS: septiembre de 1997 a agosto de 2004 (Ph.D. thesis). Universitat de Barcelona, CSIC, Universitat Politècnica de Catalunya.
- Morán, X.A.G., Estrada, M., 2005. Winter pelagic photosynthesis in the NW Mediterranean. *Deep-Sea Res. I* 52, 1806–1822.
- Morel, A., André, J., 1991. Pigment distribution and primary production in the western Mediterranean as derived and modeled from Coastal Zone Color Scanner observations. *J. Geophys. Res.* 96, 12685–12698.
- Mouriño-Carballido, B., Graña, R., Fernández, A., Bode, A., Varela, M., Domínguez, J. F., Escáñez, J., de Armas, D., Marañón, E., 2011. Importance of N<sub>2</sub> fixation versus nitrate eddy diffusion along a latitudinal transect in the Atlantic Ocean. *Limnol. Oceanogr.* 56 (3), 999–1007.
- Osborn, T.R., 1980. Estimates of the local rate of vertical diffusion from dissipation measurements. *J. Phys. Oceanogr.* 10, 83–89.
- Pascual, A., Buongiorno Nardelli, B., Larnicol, G., Emelianov, M., Gomis, D., 2002. A case of an intense anticyclonic eddy in the Balearic Sea (western Mediterranean). *J. Geophys. Res.* 107 (C11), 3183. <http://dx.doi.org/10.1029/2001JC000913>.
- Parkhill, J.-P., Maillet, G., Cullen, J.J., 2001. Fluorescence-based maximal quantum yield for PSII as a diagnostic of nutrient stress. *J. Phycol.* 37, 517–529.
- Platt, T., Gallegos, C.L., Harrison, W.G., 1980. Photoinhibition of photosynthesis in natural assemblages of marine phytoplankton. *J. Mar. Res.* 38, 687–701.
- Prandke, H., Stips, A., 1998. Test measurements with an operational microstructure-turbulence profiler: detection limit of dissipation rates. *Aquat. Sci.* 60, 191–209.
- Salat, J., Emelianov, M., Fraile, E., Latasa, M., 2013. After deep water formation: sinking and spreading but also upwelling phase? In: Proceedings of the 40th CIEM Congress, Marseille, France.
- Salat, J., Emelianov, M., López-Jurado, J.L., 2007. Atypical western Mediterranean deep water formation during winter 2005. *Rapp. Comm. Int. Mer. Médit.* 38, 197.
- Salat, J., Emelianov, M., Puig, P., Font, J., Fuda, J.-L., 2010. Winter 2009. A new step in the Western Mediterranean transition. *Rapp. Comm. Int. Mer. Médit.* 39, 174.
- Siegel, D.A., Doney, S.C., Yoder, J.A., 2002. The North Atlantic spring phytoplankton bloom and Sverdrup's critical depth hypothesis. *Science* 296, 730–733.
- Siokou-Frangou, I., Christaki, U., Mazzocchi, M.G., Montresor, M., Ribera d'Alcalá, M., Vaqué, D., Zingone, A., 2010. Plankton in the open Mediterranean Sea: a review. *Biogeosciences* 7, 1543–1586.
- Smith, R.O., Bryden, H.L., Stansfield, K., 2008. Observations of new Mediterranean deep water formation using Argo floats 2004–2006. *Ocean Sci.* 4, 133–149.
- Somot, S., Sevault, F., Déqué, M., 2006. Transient climate change scenario simulation of the Mediterranean Sea for the twenty-first century using a high-resolution ocean circulation model. *Clim. Dyn.* 27, 851–879. <http://dx.doi.org/10.1007/s00382-006-0167-z>.
- Suggest, D.J., Moore, C.M., Hickman, A.E., Geider, R.J., 2009. Interpretation of fast repetition rate (FRR) fluorescence: signatures of phytoplankton community structure versus physiological state. *Mar. Ecol. Prog. Ser.* 376, 1–19.
- Vidussi, F., Marty, J.C., Chiavérini, J., 2000. Phytoplankton pigment variations during the transition from spring bloom to oligotrophy in the northwestern Mediterranean sea. *Deep-Sea Res. I* 47, 423–445.
- Volpe, G., Nardelli, B.B., Cipollini, P., Santoleri, R., Robinson, I.S., 2012. Seasonal to interannual phytoplankton response to physical processes in the Mediterranean Sea from satellite observations. *Remote Sens. Environ.* 117, 223–235.
- Webb, W.L., Newton, M., Starr, D., 1974. Carbon dioxide exchange of *Alnus rubra*: a mathematical model. *Oecologia* 17, 281–291.
- Welshmeyer, N.A., 1994. Fluorometric analysis of chlorophyll a in the presence of chlorophyll b and phaeopigments. *Limnol. Oceanogr.* 39, 1985–1992.
- Yentsch, C.S., Menzel, D.W., 1963. A method for the determination of phytoplankton chlorophyll and phaeophytin by fluorescence. *Deep-Sea Res.* 10, 221–231.